JOURNAL OF GEOPHYSICAL RESEARCH, VOL. 106, NO. 0, PAGES 1–22, MONTH 2001

Utopia Basin, Mars: Characterization of topography and morphology and assessment of the origin and evolution of basin internal structure

Bradley J. Thomson and James W. Head III
Department of Geological Sciences, Brown University, Providence, Rhode Island, USA

Abstract. Recently obtained Mars Orbiter Laser Altimeter (MOLA) topography has permitted a new assessment of the morphology, structure, and history of Utopia Planitia. The new topographic data convincingly demonstrate that the Utopia region is an impact basin, as originally proposed by *McGill* [1989], whose major topographic expression is a circular, 1–3 km deep depression ~3200 km in diameter. Utopia Basin is the largest easily recognizable impact structure in the northern hemisphere of Mars and is the only portion of the northern lowlands that exhibits a distinct large-scale impact signature; its presence there and its ancient age verify that a significant part of the northern lowlands dates back to the Noachian period. Using slope maps derived from gridded topography, we have mapped a series of linear slope anomalies within the basin and have analyzed their origin. These features can be classified into two groups: one oriented dominantly radial to the basin and the other oriented dominantly circumferential. The circumferential features are tens of kilometers wide and hundreds of kilometers long and appear to remain relatively constant with respect to elevation. We explore end-member hypotheses (1) that the features formed by the direct action of water/ice or (2) that they are tectonic wrinkle ridges. We interpret the majority of these features to be due to tectonic deformation (primarily wrinkle-ridge formation), modified by later sedimentation associated with the emplacement of the outflow channels and the formation of the Vastitas Borealis Formation. On the basis of the characteristics of these features and their association with polygonal terrain, thumbprint terrain, smoothness of units, and evidence of sedimentary deposits, we find that our results support earlier hypotheses proposing that a significant volume of water occupied Utopia Basin during the late Hesperian period of outflow channel formation. Utopia Basin differs significantly in depth and degradation state from the deeper and fresher-appearing Hellas Basin, although the two are both Noachian in age. A significant part of this difference seems reasonably interpreted to be the result of the extensive sedimentary and volcanic infilling history of the northern lowlands.

1. Introduction

The images returned by Mariner 9 of the massive outflow channels provided the first indication that large amounts of water once flowed across the surface of Mars [*McCauley et al.*, 1972; *Masursky*, 1973; *Milton*, 1973], despite the fact that at current pressures and temperatures liquid water is not stable on the surface [*Hess et al.*, 1977; *Kieffer et al.*, 1977]. While most investigators agree that fluvial processes have operated at some time during Martian history [e.g., *Sharp and Malin*, 1975; *Carr*, 1979, 1996; *Baker*, 1982; *Mars Channel Working Group*, 1983], there is a great deal of debate about the total amount and persistence of water in the Martian hydrological cycle [*Dreibus and Wänke*, 1987; *Greeley*, 1987; *Yung et al.*, 1988; *Clifford*, 1993]. Some authors have suggested that large standing bodies of water existed at the terminus of these channels in the past [*Witbeck and Underwood*, 1983; *Jöns*, 1984, 1985, 1990; *Lucchitta et al.*, 1986; *Lucchitta*, 1993; *Parker et al.*, 1989, 1993; *Baker et al.*, 1991; *Scott et al.*, 1992, 1995]. *Parker et al.* [1989, 1993] mapped two contacts around the circumference of the northern plains and interpreted them to be shorelines, representing former highstands of an ancient northern ocean. The surface area of the northern plains contained within the outer proposed contact is about 46×10^6 km^2 [*Parker et al.*, 1993], which is slightly less than one third of the surface area of the planet. Previously, we have tested the hypothesis of a paleoocean in the northern hemisphere of Mars with the Mars Orbiter Laser Altimeter (MOLA) [*Head et al.*, 1998, 1999a]. MOLA topographic data have shown that (1) the outer proposed contact (Contact 1) ranges in elevation over almost 11 km and is not a good approximation of an equipotential line; (2) Contact 2 mapped by *Parker et al.* [1993] shows significant local deviation from a straight line in the Utopia area [*Head et al.*, 1999a, Figure 2]; and (3) the inner proposed contact better approximates an equipotential surface for the northern lowlands as a whole (mean elevation −3.76 km, standard deviation 0.56 km) [*Head et al.*, 1999a, Figure 2] than does Contact 1. The new topographic data have also revealed the extent and morphology of the two large subbasins within the northern hemisphere, the North Polar Basin and Utopia Basin. This analysis focuses on the characterization of Utopia Basin, its internal structure, and evolution.

Utopia Planitia is a large plain located in the northern lowlands of Mars (Plate 1a). It was recognized on the basis of its uniform albedo through early telescopic observations. It is an area of long-standing interest and was selected as a landing site for Viking 2 because of its high scientific significance coupled with spacecraft survivability concerns [*Masursky and Crabill*, 1976].

The Utopia region is crossed by over 1500 mapping phase MOLA tracks (prior to solar conjunction, July 2000) that have a general north-south trend. The integrated laser footprint is ~100 m in diameter, and the shot separation distance is ~300 m. Surface features covered by these tracks can be resolved with a shot-to-shot

Paper number 2000JE001355.
0148-0227/01/2000JE001355$09.00

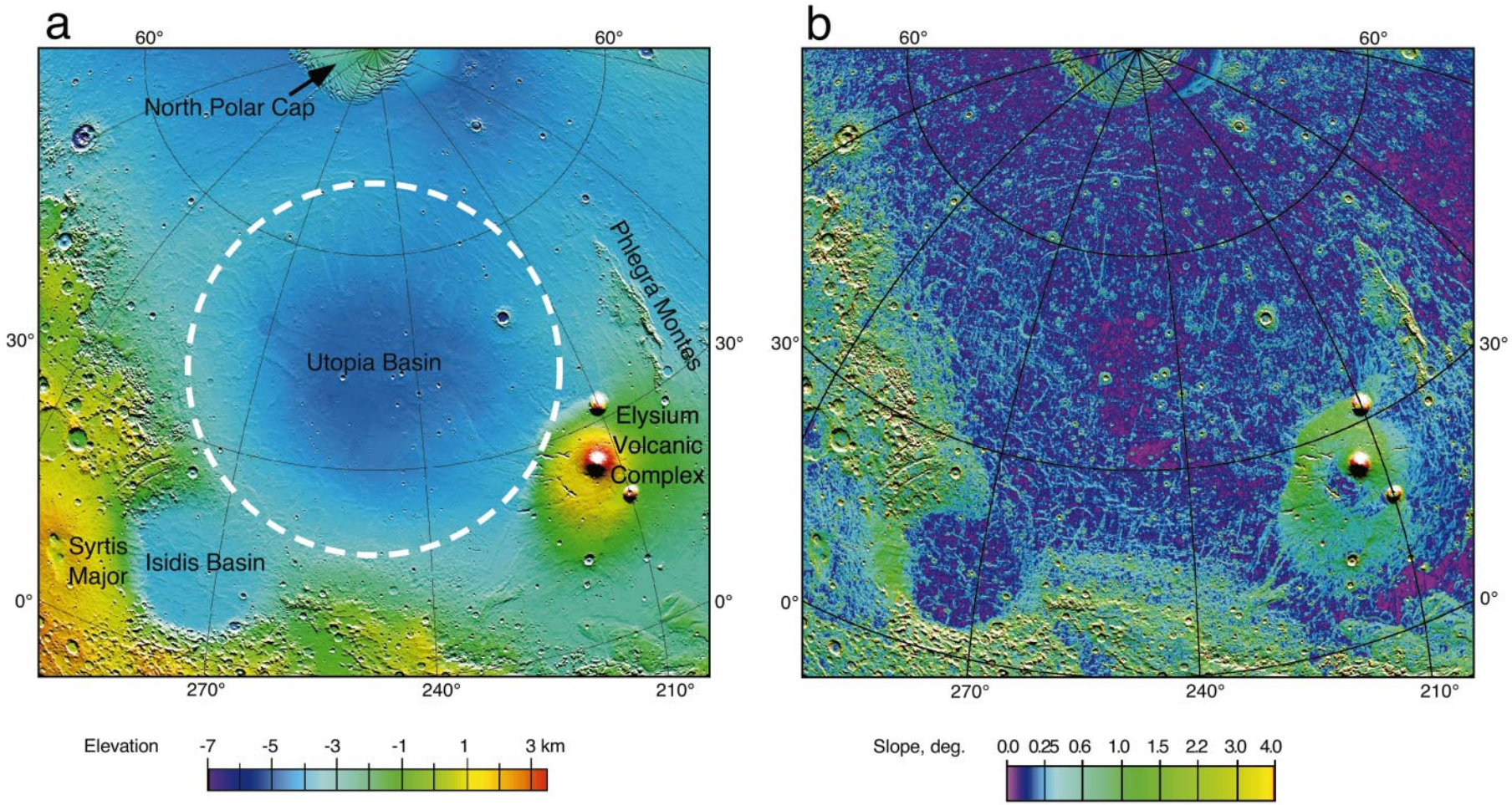

Plate 1. (a) Shaded relief map of Utopia Basin. The image is a Lambert azimuthal equal-area projection of the 1/16 degree gridded MOLA topography centered at 45°N latitude, 248°W longitude. White dashed circle outlines the present topographic rim of the basin, ~3200 km in diameter. Utopia Basin is situated on the edge of the planetary dichotomy boundary. Prominent nearby landforms are the Isidis Basin to the southwest, the Elysium volcanic complex to the southeast, and the northern layered terrain and residual ice cap visible at the top of the image. (b) Slope map of Utopia Basin. This slope map was derived from the gridded topography by fitting a plane to each pixel and the eight adjacent pixels. The slope of this plane was assigned to the center pixel. Since each pixel represents 1/16 of a degree (one degree is equal to ~59 km at the equator), the measured slope has a baseline of 11.1 km at the equator. The linear features in Utopia are visible as bands of steeper slope that stand out from the regional slope.

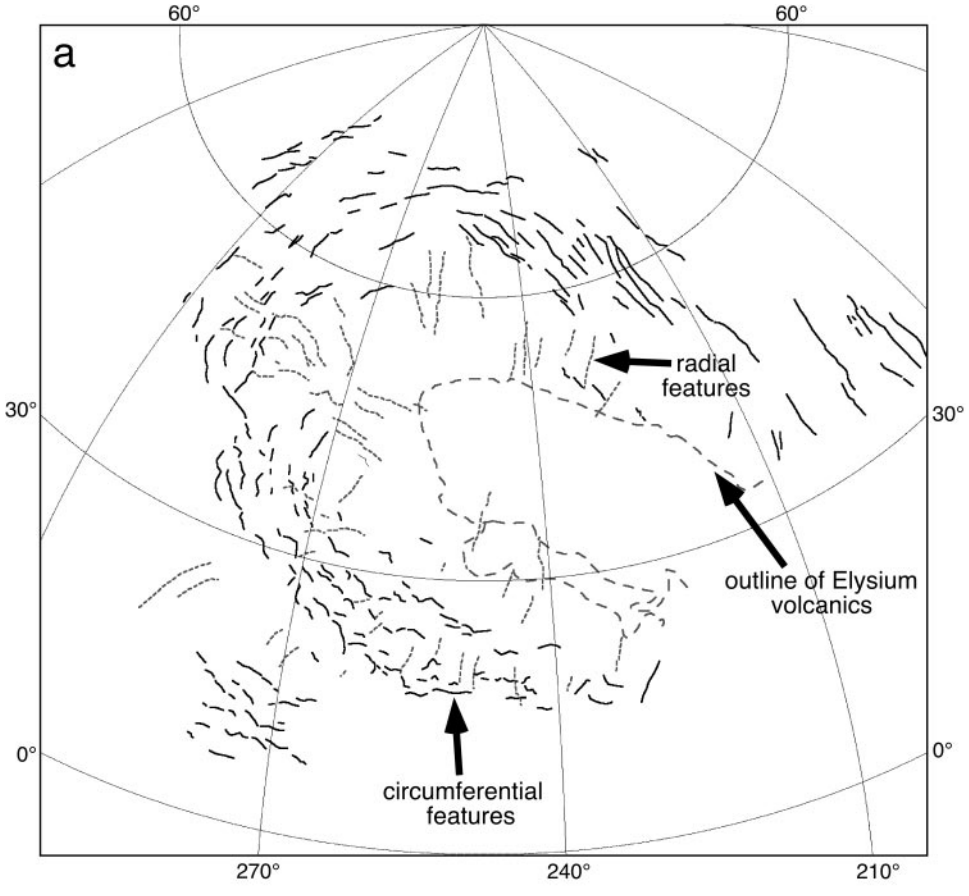

Figure 1. (a) Map showing the distribution of linear features in Utopia. Outlines of the Amazonian volcanic deposits from Elysium that fill the lowermost portion of the basin are shown as mapped by *Greeley and Guest* [1987]. Two classes of linear features are given, those with a circumferential trend (solid black lines) and those with a radial trend (short dashed lines). (b) Mars Orbiter Laser Altimeter (MOLA) altimetry profiles across the Hellas Basin and Utopia Basin for comparison.

uncertainty of ~30 cm and a cross-track uncertainty of ~13 m [*Smith et al.*, 1998, 1999]. An initial investigation of the Utopia region using the premapping phase MOLA tracks [*Thomson and Head*, 1999] revealed the presence of a circumferential terrace-like feature within the basin at an elevation of −4350 m. Other similar features were hinted at in these early orbits, although the density of the data coverage was insufficient to fully characterize them. Additional observations of terraces and benches in southern Utopia as well as an analysis of the timing of the regional slope were recently reported by *McGill* [2001].

Using the more complete mapping phase MOLA data, we have been able to document the morphology and distribution of the basin and related features. In this paper we evaluate the general topographic signature of the Utopia region, characterize the distribution and morphology of linear features and structures within the basin, and assess the potential origin of these features and their relation to the history of the basin and the possible presence of former standing bodies of water in the northern hemisphere of Mars.

2. Dimensions and Morphologic Characteristics of Utopia Planitia

Prior to MOLA topographic data, the exact dimensions of Utopia Planitia were difficult to assess because of the basin's general shallowness and subdued slopes. The new topography (Plate 1a) has shown that Utopia is far larger and more circular in planimetric outline than suggested in previous topographic maps [*Wu*, 1991; *U.S. Geological Survey*, 1993], which had elevation uncertainties of up to ±1.5 km. The Utopia region is surrounded by a variety of diverse landforms. The basin is bounded by the crustal dichotomy boundary to the south and west, by the Isidis impact basin to the southwest, by the Elysium volcanic complex to the east, and by an unnamed broad, arcuate ridge to the north (Plate 1a). This ridge forms the boundary between Utopia Basin and the North Polar Basin. The crest of this low ridge does not all lie at the same elevation, but instead dips down to a broad saddle point to the northeast. This saddle is the point of initial communication between the two subbasins in the northern hemisphere and is located at about 60°N, 237°W.

Before MOLA data were available, an impact origin of the basin was inferred by *McGill* [1989] using indirect geologic evidence. On the basis of the distribution of features such as knobs, mesas, partially buried craters, and ring fractures, *McGill* [1989] proposed that Utopia Planitia is a large, degraded impact basin. This hypothesis has now been confirmed by MOLA topographic data. The circularity, symmetry, and bowl-shaped appearance of the basin (Plate 1a, Figures 1a and 1b) strongly suggest an impact origin [*Smith et al.*, 1998, 1999]. The geographic center of the basin (taken as the center of symmetry) lies at about 45°N, 248°W. The subdued ridge on the north side of the basin can be used to define a topographic ring around the center of the basin that is ~3200 km in diameter (Plate 1a). The exact ring placement remains somewhat open to interpretation owing to the degraded nature of the basin. Other workers [*Frey et al.*, 1999] have placed a

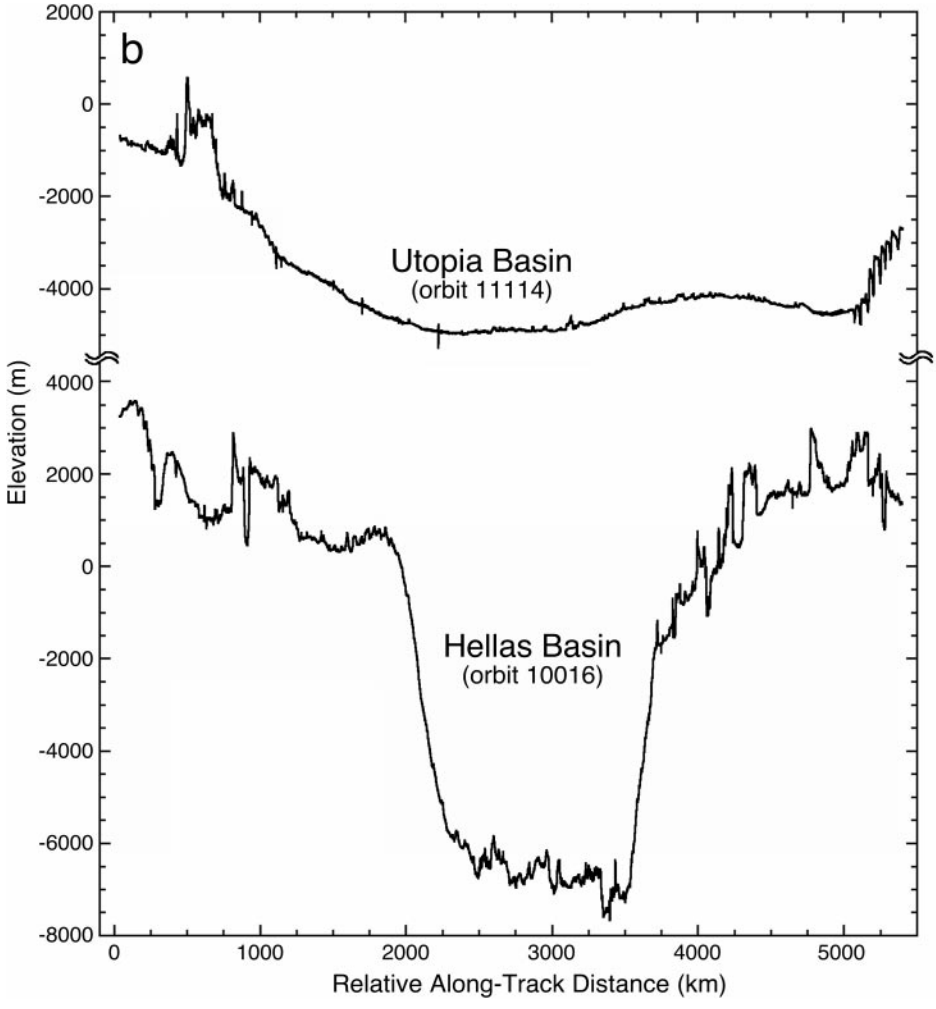

Figure 1. (continued)

similar-sized ring centered around a point that is offset from the geographic center of the basin on the basis that it appears to better fit the dichotomy boundary (H. Frey, personal communication, 1999). A circle fit to the dichotomy boundary between 240°W and 300°W has also been suggested as a possible outer ring ~4600 km in diameter [*McGill*, 1989; *Schultz and Frey*, 1990; *Frey et al.*, 1999]. Although the general trend of the Phlegra Montes corresponds to this proposed ring, there is no clear evidence of a ring with this diameter continuing into high latitudes north of the inner ring. Regardless of these discrepancies, Utopia Basin is clearly the largest easily recognizable impact structure in the northern hemisphere of Mars and is among the largest impact basins in the solar system. Although of a size comparable to the Hellas Basin (Figure 1b) and of similar age, Utopia Basin differs significantly in its depth, morphology, and structure. Gravity and topography data show that Utopia and Hellas share the characteristics of crustal thinning below the basin and annuli of thickened crust in the surroundings; however, the characteristics of Utopia point to subsequent significant volcanic and sedimentary filling *Zuber et al.*, 2000]. We now turn to assess the morphology, structure, and stratigraphy of the basin interior using the new data.

3. Interior Morphology and Structure

Parker et al. [1989, 1993] mapped a series of contacts along the margins of the northern lowlands and interpreted them to be shorelines representing highstands of a former standing body of water. *Head et al.* [1999a] analyzed the distribution of the contacts and showed that the older Contact 1 varied significantly and was not a good estimate of an equipotential line. The younger Contact 2 was shown to be closer to an equipotential line for the global average but differed considerably in several specific locations (e.g., in Tharsis, Elysium, Lyot). The widest divergence of Contact 2 occurred in Elysium [*Head et al.*, 1999a, Figure 2], where *Parker et al.* [1993] apparently mapped the edge of the younger Amazonian deposits from Elysium as Contact 2. Despite these major mapping inconsistencies and the divergence from a straight line as a function of elevation for Contact 2 in this region, *Thomson and Head* [1999] found evidence of subdued terrace-like features paralleling but below the −3760 m contour line defining the Contact 2 mean elevation globally. In addition to *Parker et al.* [1989, 1993], several other investigators had proposed that water (both liquid and ice) had played a significant role in the evolution of Utopia [e.g., *Chapman*, 1994; *Kargel et al.*, 1995; *Scott et al.*, 1992, 1995]. A logical next step in the analysis of the basin was to look for evidence of such flooding and filling of the northern hemisphere and Utopia Basin. We thus constructed a slope map derived from the gridded topographic data (Plate 1b) to enhance any low-relief, subtle topographic structures using techniques described by *Sharpton and Head* [1985, 1986] and *Head et al.* [1999b]. This slope map reveals a suite of terrace and ridge-like features that lie on the gently sloping basin walls. These linear slope anomalies are difficult to detect on topographic maps that are colored with respect to elevation because the relief of these features is often small compared to regional topographic trends.

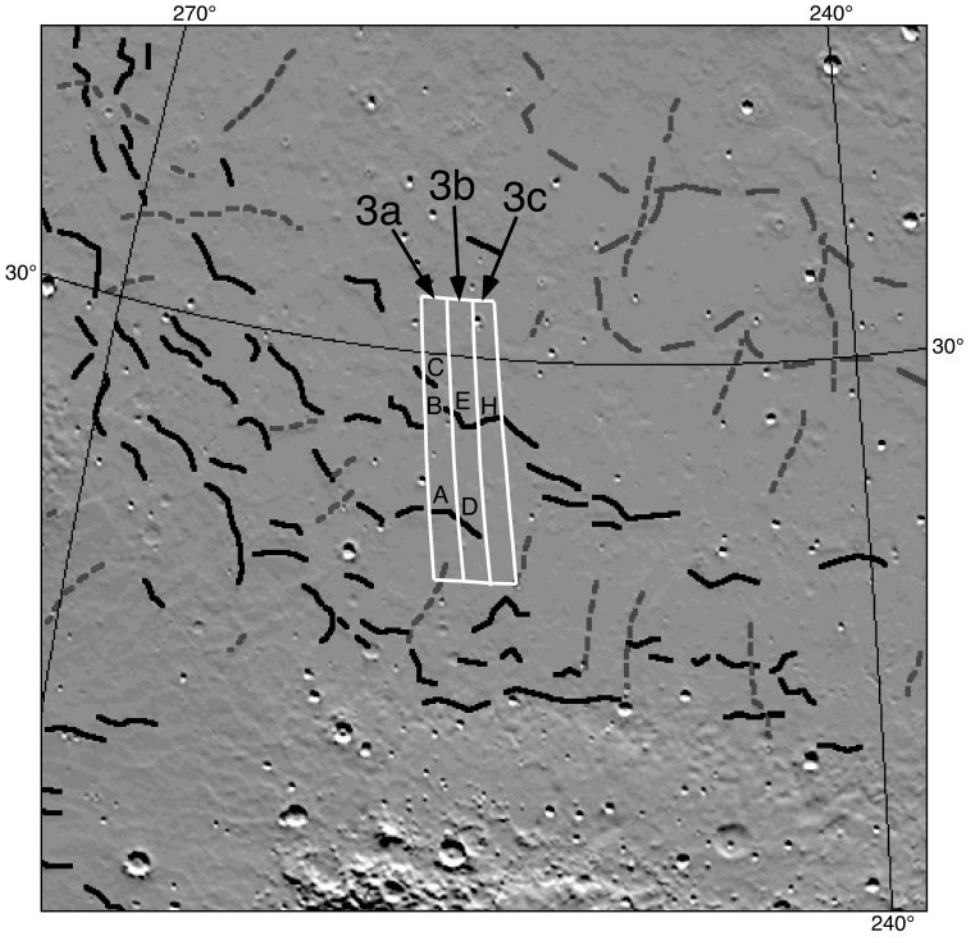

Figure 2. Location map of stacked profiles that are given in Figures 3a–3c. This map shows the mapped features shown in Figure 1 overlaying a shaded relief map. The region covered by the stacked profiles is outlined in white. Letter designations correspond to individual features labeled in Figures 3a–3c. Each outlined zone is 600 km long and ~50 km wide.

Figure 1 shows the distribution of these features we have mapped using the slope map given in Plate 1b. We have included only features greater than about 25–30 km long whose steepest surface is at least 2–3 times the regional slope. One limitation of this mapping technique is that smaller details are lost to the averaging of the gridded topography. The slope map is insensitive to short-wavelength surface undulations that are smaller than ~10 km. Analysis of individual profiles in the following sections indicates that there are, however, additional fine-scale lineations that are not evident in the slope map. Two classes of features have been identified in the basin: those that follow a circumferential trend to the basin center and those that lie along radial trends (the class of radial features includes both radial and subradial features).

4. Characterization of Circumferential Features in Southern Utopia

The circumferential features are manifested in Plate 1b as breaks in the regional slope. Examples of individual MOLA profiles that cross these features are given in Figures 3a–3c. These particular features were chosen because they trend nearly perpendicular to the MOLA tracks. The location of these three sets of stacked profiles is given in Figure 2. Each set covers an area 600 km long by ~50 km wide. As shown in Figure 2, there are portions of three mapped circumferential features that lie in the area covered by the profiles in Figure 3a. In Figure 3a the locations of the features that are crossed are indicated by the shaded regions and the dashed vertical lines. These profiles are arranged top down from west to east, and the actual distance between the ground tracks of the profiles varies from ~3 km to 14 km. The feature marked A lies at an elevation of about −3850 m and appears as a small ridge with a steeper side that faces downhill. As one moves east (down the stack of profiles), one can see that the feature gradually broadens from ~35–40 km wide to ~50–60 km wide and breaks into a pair of notch-like features as indicated by the dashed lines. The features labeled B (at about −4050 m) and C (the upper ridge is approximately −4100 m, and the lower ridge is approximately −4200m) both consist of double ridges, each of which is about 40–50 km wide. The gap in the dashed vertical lines that delineate features B and C in Figure 3a between orbits 11,737 and 13,363 reflects the discontinuity of the features in the location map (Figure 2). The east-west spacing between these two orbits is ~12 km.

Figure 3b is a set of stacked profiles that lie east of those shown in Figure 3a. Of the three sets of features that are highlighted in this stacked profile, only two are mapped in Figure 2. Feature D (−3900 m), a low ridge-like feature composed of two parts, becomes less apparent as one moves down the stack. Figure 2 shows this mapped feature terminating partway across the outlined region. The middle feature, labeled E (−4100 m), is evident throughout this set of profiles, and in some profiles a second feature is evident immediately below it. Feature F (−4450 m) does not correspond to a mapped feature, although it is visible as a

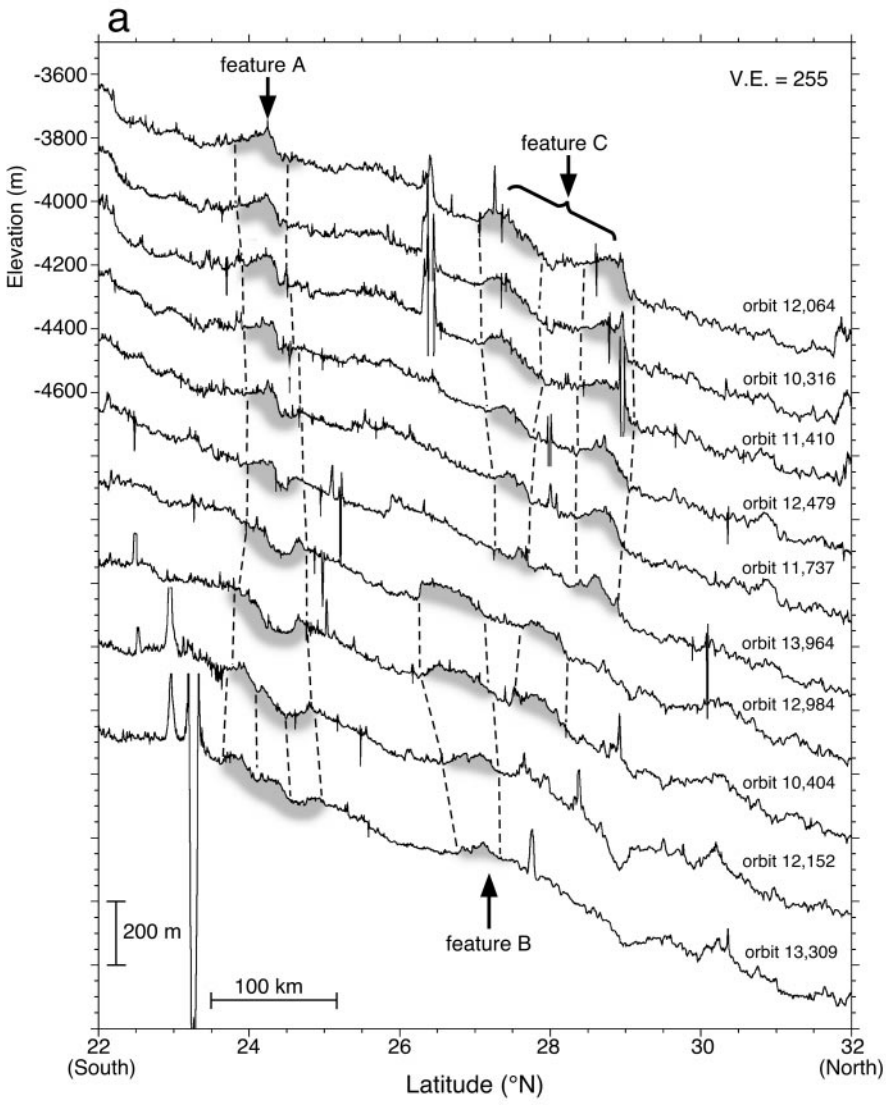

Figure 3. Stacked profiles showing relative elevation versus latitude of 30 MOLA profiles covering the areas outlined in Figure 2. The profiles within each stack are arranged top down from west to east. Each of the elevations given along the upper left axis of each figure is the true elevation the uppermost profile in the stack. The actual distance between the ground tracks of these profiles varies between about 3 km and 14 km. The floors of some craters have been removed from these profiles to reduce overlap for clarity. (a) As evident in Figure 2, portions of three mapped circumferential features are crossed by this set of profiles and are labeled features A–C. The expression of these features in the individual profiles is highlighted with shading and vertical dashed lines. The dashed lines indicate a clear continuation of a single linear feature across multiple profiles, and each set has been assigned a letter designation. (b) Stacked profiles that lie immediately east of the set shown in Figure 3a. As indicated in Figure 2, there are two mapped circumferential features that are crossed by this set of profiles, although three linear slope anomalies are evident in the profiles. These are indicated by vertical dashed lines and are marked features D–F. See text for further discussion. (c) Stacked profiles lying east of the set shown in Figure 3b. Of the three segment groupings delineated by the dashed lines, only feature H was mapped in Figure 1. Features G and I, although discernable in the profiles, appeared less prominent in the slope map used to construct Figure 1.

distinct break in slope in each profile. Traces of it are also visible in the preceding stacked profile, Figure 3a. This feature was not included in the map in Figure 1 because it is not visually prominent in the slope map (Plate 1b). Thus it is clear that there are additional linear slope anomalies that are continuous across many tens of kilometers that are below the detection limit of the slope map. The final stacked profile in this set, shown in Figure 3c, lies to the east of the profiles shown in Figure 3b. As shown in Figure 2, only one mapped circumferential feature crosses the outlined region. This feature, labeled feature H (−4200 m), is crossed near the middle of the profiles, near 27.5°N latitude. However, other features (marked as features G, approximately −3900 m elevation, and I, approximately −4500 m elevation) are highlighted in the stacked profile both above and below this mapped feature that stand out in the profiles but not in the slope map. Lining up all three sets of stacked profiles in Figures 3a–3c, one can observe a general continuity between them. In each set, there is evidence for an upper, middle, and lower set of features that each occur in the same elevation range. From this we can conclude that these circumferential features are more consistent and continuous than they appear in

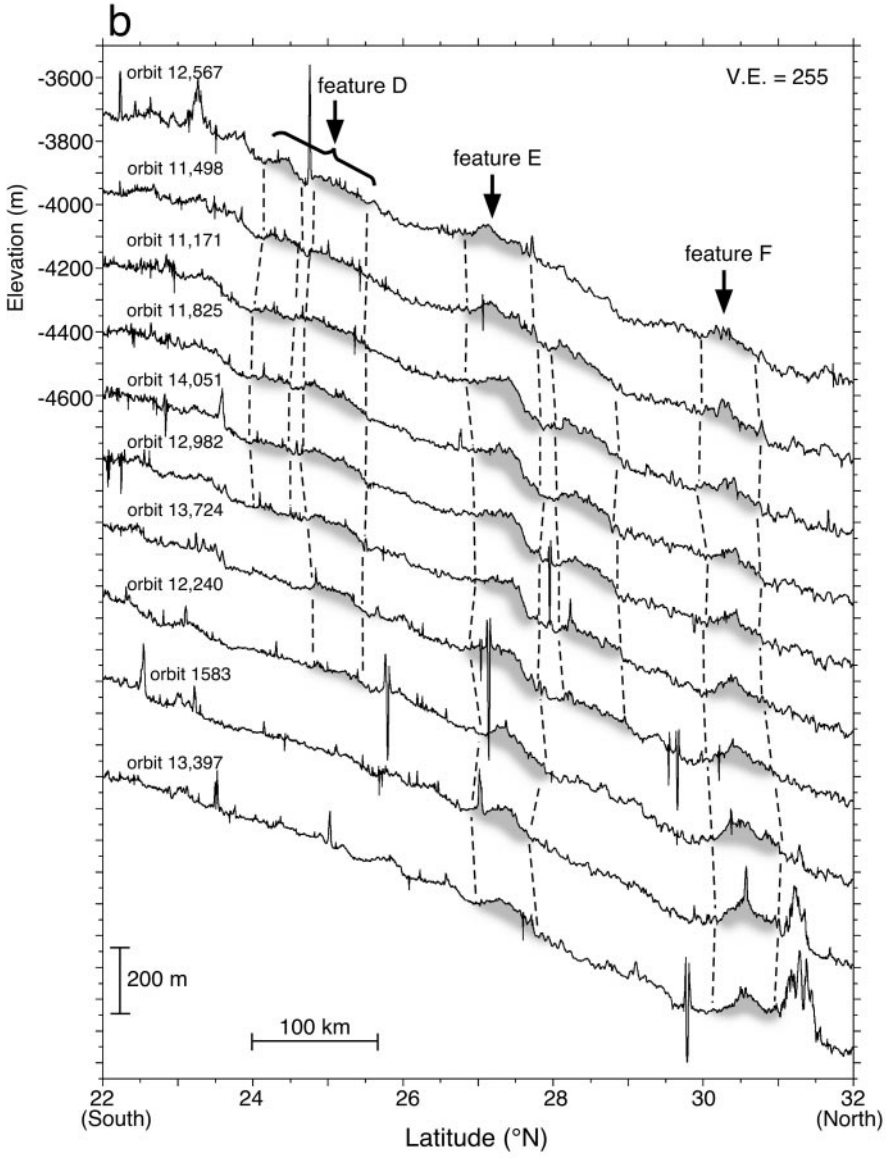

Figure 3. (continued)

Figure 1 and are generally consistent over a lateral distance of at least 120 km.

On the basis of these 30 profiles given in Figures 3a–3c, we have documented 48 individual crossings of features that were mapped in Figure 1 and have detected 27 additional crossings of linear slope anomalies that were not included in our mapping. Comparing the characteristics of each of the 75 crossings, we have subclassified these circumferential features into two groups: bench-type features and ridge-type features. Examples of these subtypes are given in Figure 4. Bench-type features consist of a large bench or platform ~20–50 km in width where the cross-platform gradient flattens to an almost level surface. This is followed by a steeper face ~10–15 km wide. It is this steeper face that stands out in the slope maps. These steeper segments typically have slopes that are 3–7 times the regional slope, or 0.25°–0.60°. The overall regional slope within the basin is quite shallow, typically on the order of 0.1°. Other mapped features possess a small symmetrical or asymmetrical ridge, and hence we have designated them as ridge-type features. Here, instead of the regional slope flattening out to a level plane, it reverses and forms a small ridge (Figure 4). This ridge is typically ~10–80 m above the dip that precedes the ridge. The downslope side of the ridge forms a steeper face similar to the steep face of the bench-type features, although the degree of steepness is less. These steep faces commonly have slopes ~0.2°–0.4°. The upslope half of the ridge is ~5–25 km wide, while the steeper downslope face is wider, typically up to twice as wide.

The sets of features that have been grouped together with dashed vertical lines in Figures 3a–3c exhibit some degree of morphologic variation along their strike from profile to profile. For example, feature A (−3850 m) in Figure 3a appears as a ridge-like feature in the first five successive profiles, after which it appears more like a bench-type feature. Feature E (−4100 m) in Figure 3b transitions from a ridge-type to a bench-type and then back to a ridge-type moving down the stack. Feature F (−4450 m) in Figure 3b appears as a ridge-like feature throughout, but the height of the ridge varies from ~50 m to over 100 m. In addition to these morphologic variations, the elevation range over which these features occur is relatively narrow but displays some trends. For example, the top of the steeper face of the feature centered at ~27.5° N latitude (labeled features B, E, and H in Figures 3a, 3b, and 3c, respectively) that is crossed by the profiles in Figures 3a–3c lies at a mean elevation of −4107 m with a standard deviation of 56 m. It

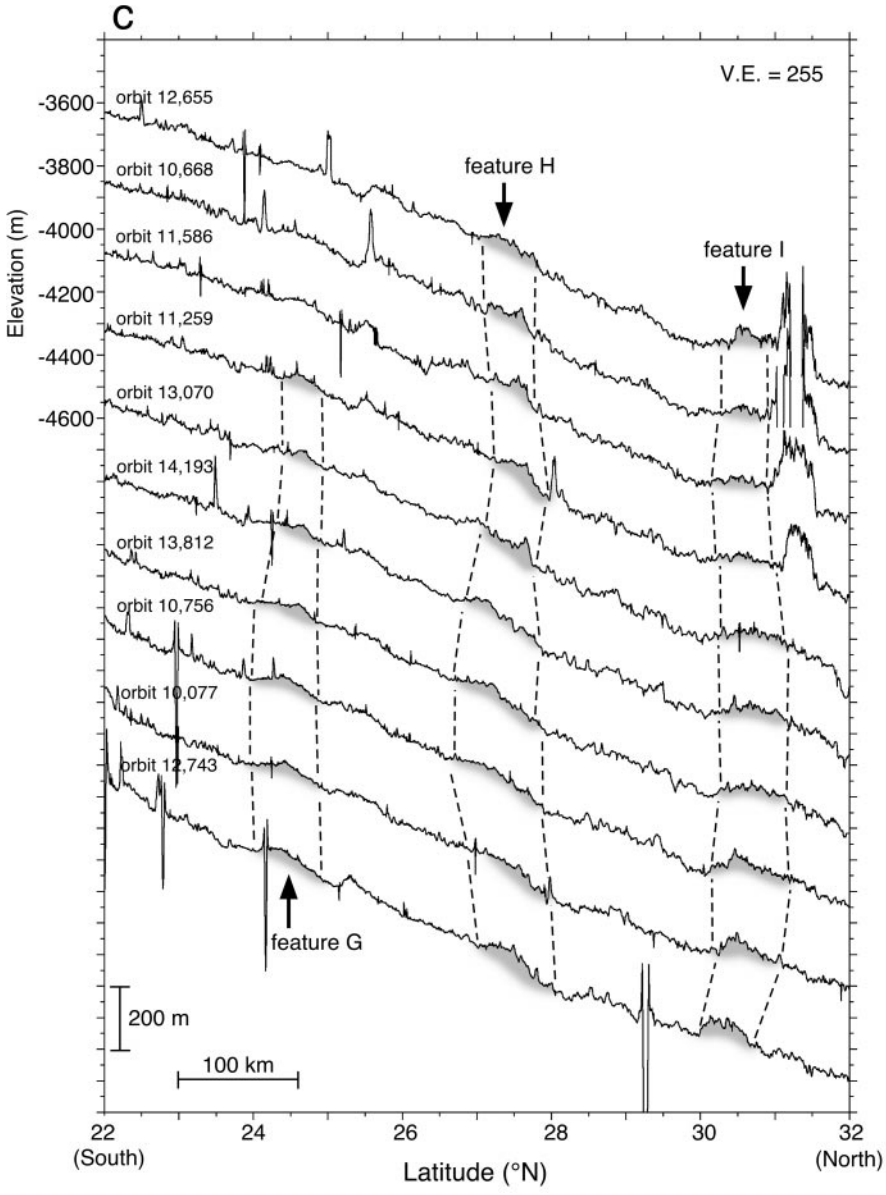

Figure 3. (continued)

lies within ±90 m of a constant elevation over a horizontal extent of over 120 km but shows a specific downslope trend from west to east (Figure 4b).

To summarize these results, we observe that individual circumferential features are many tens to hundreds of kilometers in length. A close examination of the individual profiles demonstrates that additional linear slope anomalies are evident in the profiles that are not apparent in the slope map. These features have a variable morphology and exhibit a relatively narrow range of elevations over a broad horizontal extent but often show consistent along-strike trends slightly oblique to contour lines.

5. Characterization of Circumferential Features in Northern Utopia

The location of a set of stacked profiles which crosses circumferential features on the northern rim of Utopia Basin is shown in Figure 5. The region outlined in black is 600 km long by 20 km wide. The individual profiles in this zone are shown in Figure 6 arranged top down from west to east. The spacing between the ground tracks of these profiles varies between about 1 and 3 km. The dashed vertical lines in Figure 6 delineate crossings of four circumferential features, of which three are mapped in Figure 5. The northernmost feature appears to terminate before the boundary of the outlined region in Figure 5, but the individual profiles in Figure 6 show that there is some trace of it (feature M) that extends across the outlined region. Moving down the stack of profiles in Figure 6, feature M (−4150 m) appears to transition from an asymmetrical ridge to a high-relief, peaked symmetrical ridge. Feature L (−4000 m) occurs at the top of the broad ridge crest that forms the topographic boundary between the Utopia and North Polar Basins. It appears as a complex ridge with a variable morphology. Features J and K also exhibit a ridge-like morphology. There are a number of additional features that lie between the highlighted sets of features that exhibit some consistency across the stack. In general, circumferential features on the northern rim of Utopia appear more ridge-like then bench-like. Their overall relief of ∼40 m to 170 m is

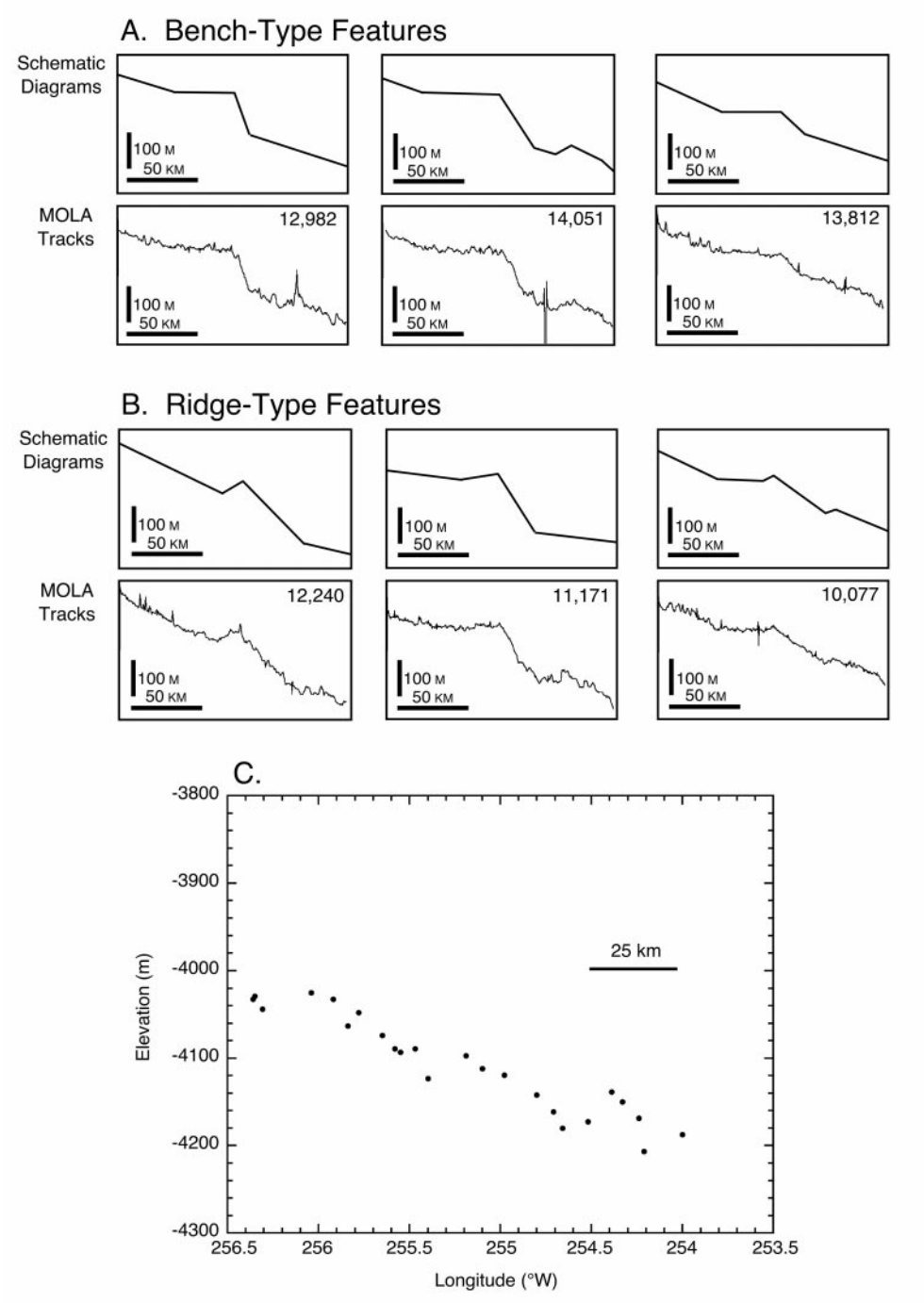

Figure 4. Portions of topographic profiles given in Figure 3 with schematic diagrams. (a) Examples of bench-type features. This feature consists of a broad platform where the cross-platform gradient is nearly level, followed by a steeper foreslope. In these examples the platform varies between 34 to 50 km in width, with foreslopes ranging between 0.25° and 0.60°. The regional slopes are in the range 0.079°–0.090°, making the foreslopes 3.1–6.6 times the regional slope. (b) Examples of ridge-type features. A variation of the bench-type feature, this feature has a small ridge that may be preceded by a flat area or shallow depression. The ridge is asymmetrical, and the steepest side faces the downhill direction. The ridge heights vary from 11.8 to 76.1 m, and the back half of the ridges varies from 5 to 25 km in width. Regional slopes are 0.087°–0.106°, while the foreslopes range from 0.161° to 0.426° (1.8–4.1 times the regional slope). (c) Elevation of the feature centered at 27.5°N latitude (labeled features B, E, and H in Figures 3a, 3b, and 3c, respectively) as a function of lateral distance in the basin.

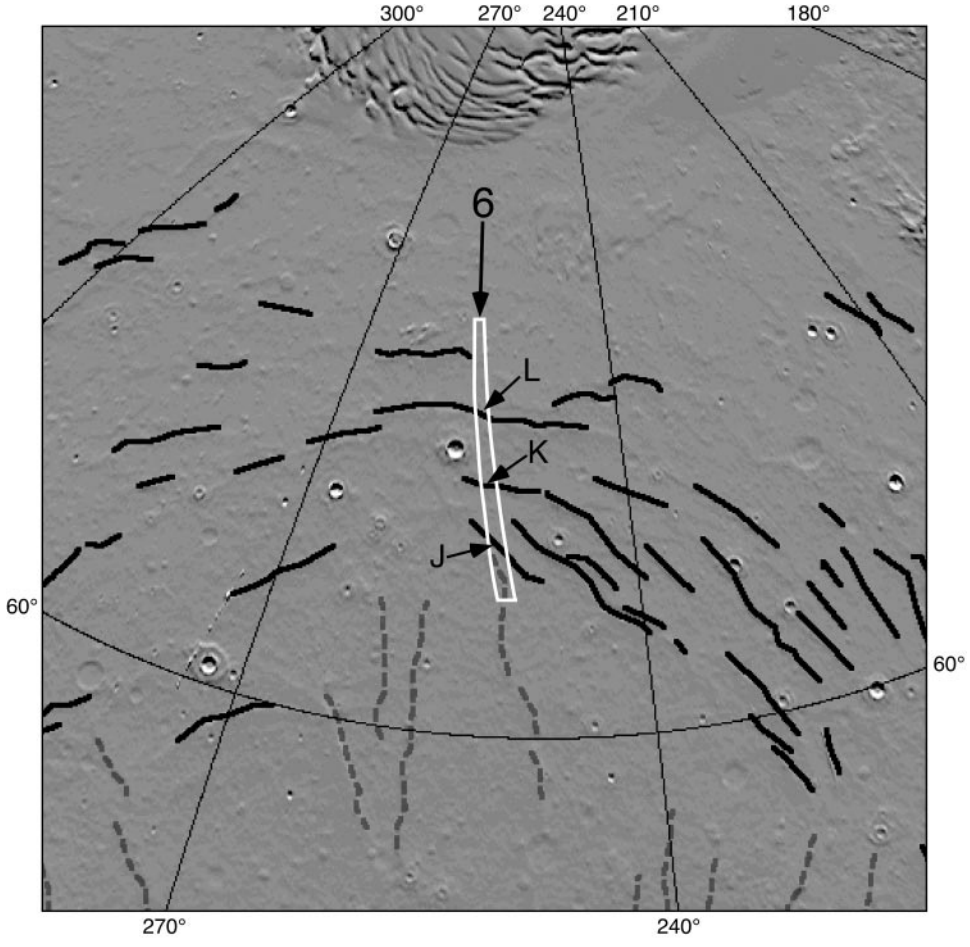

Figure 5. Location of stacked profiles shown in Figure 6. This map shows the mapped features shown in Figure 1 overlaying a shaded relief map. The region covered by the stacked profile is outlined in white. The outlined area is ~600 km long by 20 km wide, and it is located on the northern rim of Utopia Basin. Letter designations correspond to individual features labeled in Figure 6.

typically greater than the relief of ridge-like circumferential features in southern Utopia shown in Figures 3a–3c.

6. Characterization of Radial Features

Similar to circumferential features, radial features also stand out from the regional slope shown in Plate 1b. Their distribution is shown in Figure 1. They are distinguished from the circumferential features on the basis of their radial trend. In the northern portion of the basin, radial features occur primarily below the circumferential features. In the southern and eastern portions of the rim, radial features occur both in and below the zone of circumferential features. The location of a subset of these features examined in detail is given in Figure 7. These radial features lie on the floor of the basin near a large ghost crater (Plate 1b). Figure 8 shows a stack of six profiles that cross three of these features. As these individual profiles show, the general shape of these features is that of an asymmetrical ridge with a steep foreslope and a shallower backslope. These ridges range from 80 to 180 m in height and 30 to 60 km in total width. The ridges shown here are representative of the rest of the radial features present in the basin and are somewhat similar in appearance to the ridge-type feature shown in Figure 4. There are some distinctions that can be made between the two, however. The relief of these features is generally greater than the circumferential features highlighted in the previous profiles (Figures 3a–3c and 6), and their appearance is more peaked (greater height/width ratio). The steep foreslopes on some of these radial features range from 0.3° to 0.6°, similar to the foreslopes of circumferential ridges, while other radial features are steeper and have a range of slopes from 0.4° to 1.9°. In contrast to the circumferential ridges, the steepest side of the ridge does not consistently face downhill. In general, these radial features appear similar to wrinkle ridges in terms of their morphology and distribution [*Plescia*, 1993; *Watters*, 1993; *Head et al.*, 2001a, 2001b; *Head and Kreslavsky*, 2000]. Their presence indicates that the upper layers of the surface of Utopia have been subjected to a compressive azimuthal or hoop stress, probably as a result of loading [*Banerdt et al.*, 1992].

7. Distribution of Linear Features

Linear features within Utopia Basin appear in a variety of geologic units, including members of the Vastitas Borealis Formation (Hvm, Hvk, and Hvr), knobby plains material (Apk), and smooth plains material (Aps) [*Greeley and Guest*, 1987]. Both radial and circumferential features are not prominent above an elevation of −3000 m, and circumferential features are not readily apparent below an elevation of about −4350 m. These bounding contours have been superimposed over the mapped distribution of linear features (Figure 9). The upper extent of these features lies between the mean elevations [*Head et al.*, 1999a] of the two contacts of the northern ocean proposed by *Parker et al.* [1993].

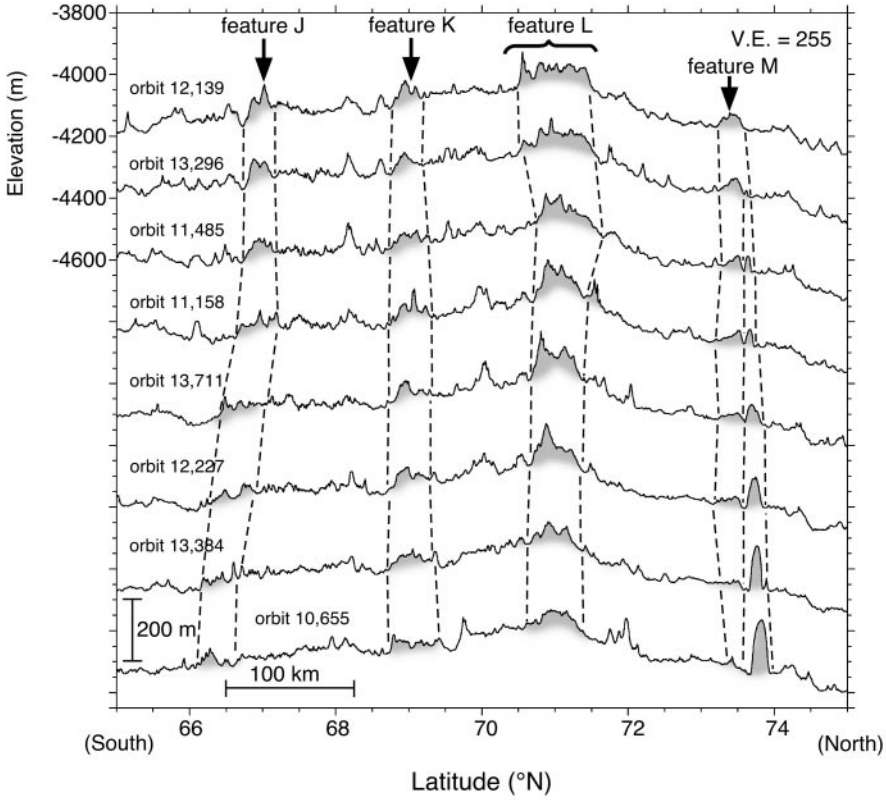

Figure 6. Stacked profiles showing relative elevation versus latitude of eight MOLA profiles in the region outlined in Figure 5. The profiles within the stack are arranged top down from west to east. The elevations given along the upper left axis are the actual elevations of the uppermost profile in the stack. The actual distance between the ground tracks of these profiles varies between about 1.5 km and 4 km.

The lower termination of the circumferential features coincides with the onset of the polygonal terrain as mapped by *McGill* [1989] (Figure 9). Recent MOLA measurements of the polygonal terrain [*Hiesinger and Head*, 2000] have confirmed that polygonal terrain in southern Utopia starts at about the −4350 m level. One of the stratigraphic relationships evident is a radial feature that appears to underlie the Amazonian-aged volcanic units that occur in the lowermost portions of Utopia Basin (Figure 9). The ridge can be clearly seen outside of the volcanic deposit and appears to continue beneath and be mantled by the unit. As the crater retention age of these volcanic deposits is early Amazonian [*Greeley and Guest*, 1987], these radial features are likely Late Hesperian or older.

8. Possible Formation Mechanisms of Linear Features

There are numerous possible explanations for the linear features described, including degraded basin-related impact structures; mass-wasting features such as gelifluction lobes and benches; tectonic features related to loading by sedimentary, volcanic, or massive relict ice deposits; glacial features such as recessional moraines; open water features such as wave-cut terraces and benches; and features related to ice-dominated bodies of water such as ice-pushed ridges or strandflats. Each of these possible formation mechanisms is discussed below.

8.1. Impact Structures

Complex craters typically exhibit wall terraces that result from collapse of the transient cavity. At the basin scale a series of concentric rings develop which consist of large inward facing scarps [*Melosh*, 1989] that are manifested as jagged structural blocks and massifs. Several characteristics of the circumferential features argue against them being primary impact features. These include their lateral continuity and subdued nature, their distribution, and the highly degraded nature of the basin. First, the terraces and scarps that form during the impact process are not necessarily constant with respect to elevation. On the Moon, basin rings appear as broken, jagged mountain ridges [*Spudis*, 1993]. Second, measurements of the spacing of basin rings show that they appear to conform to a characteristic spacing relationship, namely $\sqrt{2}$ [*Hartmann and Wood*, 1962; *Baldwin*, 1963; *Wood and Head*, 1976; *Pike and Spudis*, 1987]. Although an individual ring can bifurcate and appear as a closely spaced double ring, these still generally conform to a characteristic spacing and are not found distributed across a wide zone. The only analogous distribution of basin ring structures occurs on the icy satellites of the outer planets, such as the Valhalla structure on Callisto. This structure may have hundreds of rings, but they appear to face outward, not inward as lunar rings do [*McKinnon and Melosh*, 1980; *Greeley et al.*, 2000]. The morphology and distribution of the circumferential features within Utopia Basin do not match any impact-related structures found in other basins [e.g., *Wilhelms*, 1973; *Schultz and Frey*, 1990]. The highly degraded state of the basin also argues against the retention of any subtle primary impact features. Mars Global Surveyor (MGS) gravity/topography data show that there is a several hundred mGal positive free-air gravity anomaly centered in Utopia, which is consistent with a substantial thickness of fill [*Zuber et al.*, 2000]. The preservation of any subtle primary impact features beneath such fill seems unlikely.

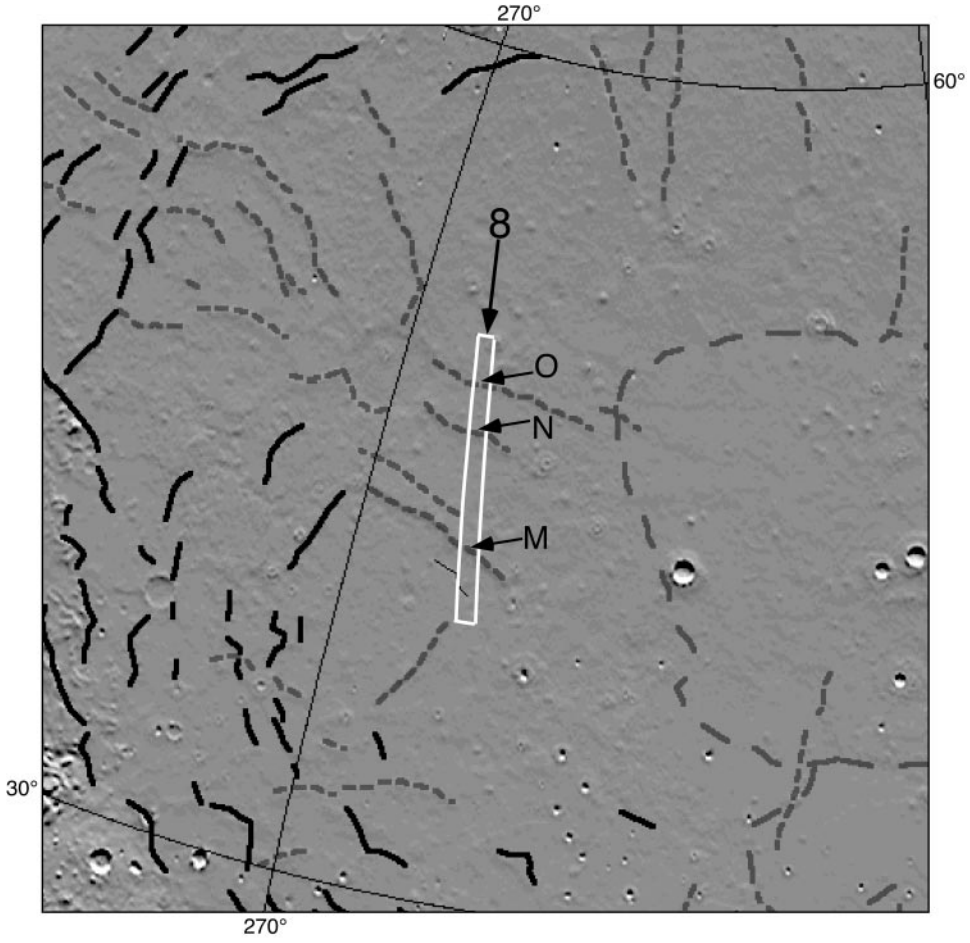

Figure 7. Location map of stacked profiles shown in Figure 8. This map shows the mapped features shown in Figure 1 overlaying a shaded relief map. The region covered by the stacked profile is outlined in white. It is ~600 km long by 42 km wide. Letter designations correspond to individual features labeled in Figure 8.

A more likely scenario is that the concentric and radial structures are related to the processes associated with basin impact modification. Comparison of the altimetric profiles for Utopia Basin and the more well preserved Hellas Basin (Figure 1b) shows that Utopia must have experienced significant modification and filling. Typical processes of modification include viscous relaxation, which is wavelength-dependent and tends to modify long-wavelength topography while preserving short-wavelength topography. Subsequent impact bombardment and sedimentary infill tend to both reduce long-wavelength topography and degrade and destroy short-wavelength topography. Volcanic infilling, as observed in the lunar maria, reduces long-wavelength topography substantially and often isolates short-wavelength topography (for example, basin ring structures) by embayment and flooding. Infilling processes also introduce a load in the basin, and the accommodation of the lithosphere to that load can result in the formation of concentric and radial wrinkle-ridge structures [e.g., *Solomon and Head*, 1979]. In some cases the concentric wrinkle-ridge structures may represent an approximation of the location of one of the buried basin rings [e.g., *Solomon and Head*, 1980]. The very high degree of modification of Utopia Basin indicated by the topography (see Figure 1b), gravity [*Zuber et al.*, 2000] data, and geological history [*Greeley and Guest*, 1987; *McGill*, 1989; *Kreslavsky and Head*, 2001] strongly suggests that the circumferential and radial features may be linked to secondary structures associated with basin modification processes, not primary impact-related features.

8.2. Mass-Wasting Features

There have been widespread inferences of near-surface ice in the Martian crust [e.g., *Carr and Schaber*, 1977; *Squyres*, 1979 *Squyres and Carr*, 1986]. Features such as lobate debris aprons, lineated valley fill, and other terrain-softening features suggest the presence of near-surface ice, although the exact mechanism of ice incorporation is not clear. One type of mass-wasting landform that is observed in terrestrial cold-climate regions is a gelifluction feature, examples of which are lobes and benches. These mass-wasting features occur from a combination of frost heaving and gelifluction. Gelifluction is a type of solifluction that occurs where a permafrost layer prevents the drainage of surface water [*Baulig*, 1957]. The upper layers in the active zone can become water saturated and are subject to viscous flow. Operating in concert with gelifluction is frost heaving, which is the ratchet-like downslope movement of saturated debris initiated by freeze-thaw cycles [*Washburn*, 1967]. Could a similar process on Mars produce the circumferential features in Utopia? The limiting factors of such a process operating on Mars would be the presence of near-surface water and a repetitive freeze-thaw cycle. The canonical view has been that given the severe limitations of the present climatic environment

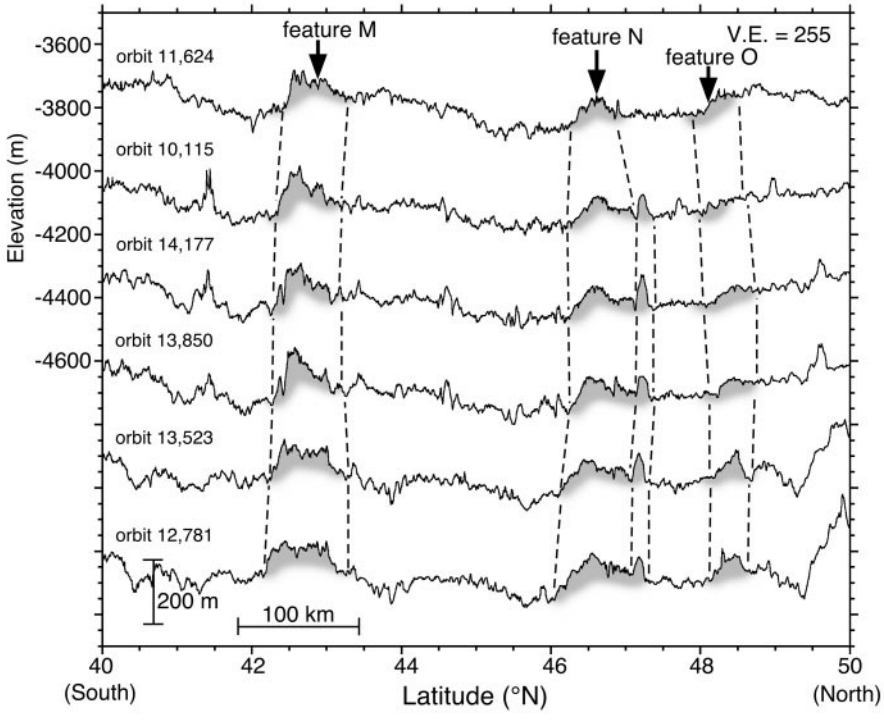

Figure 8. Stacked profiles showing relative elevation versus latitude of six MOLA profiles in the region outlined in Figure 7. The profiles within the stack are arranged top down from west to east. The elevations given along the upper left axis are the actual elevations of the uppermost profile in the stack. The actual distance between the ground tracks of these profiles varies between about 5 km and 10 km. There are three radial features crossed by this set of profiles, whose locations are indicated with shading and vertical dashed lines. Most of these features are visually prominent and clearly stand out from smaller-scale undulations in the profiles. See text for further discussion.

on Mars, seasonal temperature variations are unlikely to induce a phase transition in H_2O ice [*Coradini and Flamini*, 1979]. Recent Mars Orbiter Camera (MOC) observations, however, show evidence for recent water seepage and surface runoff [*Malin and Edgett*, 2000], indicating the possible presence of liquid water at shallow depths. These seepage features are of limited size and geographic distribution, suggesting isolated source regions. The implications of these features for the planet-wide abundance of liquid water at shallow depths are not known.

Because long-period temperature fluctuations are less attenuated with depth than shorter-period fluctuations, some have suggested that obliquity-driven variations in insolation may create extremely long period freeze-thaw cycles [*Sagan et al.*, 1973; *Ward et al.*, 1974; *Coradini and Flamini*, 1979]. *Mellon and Jakosky* [1995] examined the effects due to moderate variations in obliquity (<35°) and found that the top few meters of regolith experienced a cyclic inflation and deflation on a timescale of 10^5–10^6 years that would likely have an effect similar to a frost-heave cycle on Earth. However, the horizontal scale of geomorphic features produced by this desiccation would be expected to be of the same order as the depth of desiccation, ~1–2 m [*Mellon and Jakosky*, 1995]. Thus moderate obliquity variations are likely to be insufficient to explain the magnitude of the circumferential features observed in Utopia, which can be up to 60 km wide. It is possible that larger obliquity excursions may allow for larger geomorphic features, but the effects of these excursions have yet to be modeled in detail.

An additional consideration is the necessity to have such processes operate on extremely low slopes (~2 m/km, 0.1°) over large horizontal distances. Theoretical analyses of ice-enhanced creep rates under Martian conditions by *Zimbelman et al.* [1989] suggest that near-surface creep is precluded on slopes less than ~10°.

8.3. Tectonic Features

Features that possess a circumferential trend can also form through tectonic processes. For example, wrinkle ridges form in response to compressional stresses in the upper layers of the surface [e.g., *Plescia*, 1993; *Watters*, 1993]. They often result from the isostatic adjustment of loads within basins, such as the wrinkle ridges that are common on the lunar maria [*Solomon and Head*, 1979]. If the area over which a load is distributed is large relative to the curvature of the planet and the thickness of the elastic lithosphere, a spherical shell model can be used to describe the effects [*Banerdt et al.*, 1992]. A load on a spherical surface results in both compressional radial and azimuthal stresses, which can produce radial and circumferential wrinkle ridges. The possible loads include sediments, volcanic plains, lahar-like deposits from Elysium, the water/ice of a northern ocean, and massive relict ice deposits. Thus it is possible that tectonic features could match the distribution of features observed in Utopia.

Additional observations made with MOLA topography data support the presence of tectonic features in the northern lowlands [*Head et al.*, 2001a, 2001b; *Head and Kreslavsky*, 2000; *Kreslavsky and Head*, 2001; *Withers and Neumann*, 2001]. *Withers and Neumann* [2001] have proposed that features associated with the basin margin in Utopia and the northern flanks of Alba are primary tectonic structures. Basin-wide observations made with detrended gridded topography have revealed an extensive system of ridge and arch-like structures distributed throughout the northern lowlands [*Head et al.*, 2001a, 2001b; *Head and Kreslavsky*, 2000]. The gridded topography was detrended by applying a

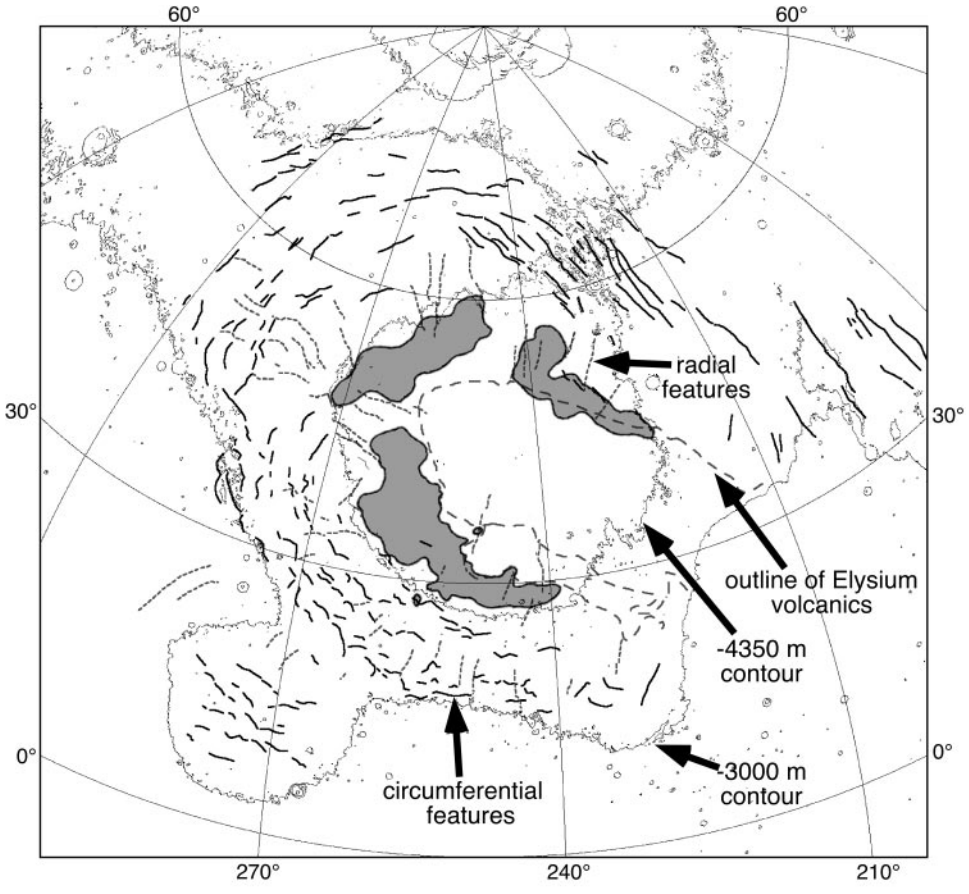

Figure 9. Map showing distribution of linear features from Figure 1. Shaded regions show the locations of polygonal terrain as mapped by *McGill* [1989]. Also included are the −3000 m and −4350 m contours, which are the approximate upper and lower boundaries of the zone containing circumferential linear features.

long-wavelength filter to remove regional topographic trends, thus highlighting small-scale features such as ridges. Observations using these data suggest that the northern lowlands are underlain by a regional unit (Hr, Hesperian ridged plains [*Kreslavsky and Head*, 2001]) containing a basin-wide system of subparallel wrinkle ridges and arches [*Head et al.*, 2001a, 2001b]. These features are similar to many of the features described in this work. The density of craters superposed on this unit suggests an Early Hesperian age [*Kreslavsky and Head*, 2001], and the unit appears to be laterally contiguous with early Hesperian ridged plains in the southern uplands. The general trend and orientation of these structures appear to be controlled by regional, circum-Tharsis stresses and local impact basin-related deformation. The spacing and height of the ridges differ, however, from ridges typical of the Hesperian-aged ridged plains outside of the northern lowlands; ridges in the northern lowlands are typically more widely spaced and lower in height. These trends, together with the morphology of partially buried craters, suggest that the wrinkle ridges are blanketed by a sedimentary unit (the Vastitas Borealis Formation) that covers the regional ridged plains with an average minimum thickness of ∼100 m [*Head and Kreslavsky*, 2000; *Head et al.*, 2001a, 2001b; *Kreslavsky and Head*, 2001].

One difference between wrinkle ridges and the circumferential features mapped in this work in Utopia is that wrinkle ridges typically exhibit an asymmetrical ridge in cross section. They do not generally match the bench-like morphology exhibited by some of the circumferential features (Figure 4). In addition, wrinkle ridges often vary with respect to elevation and are commonly broken into en echelon, discontinuous segments [*Watters and Maxwell*, 1986; *Golombek et al.*, 1991; *Watters*, 1991]. The characteristics of the circumferential features in Utopia suggest that they are not simply unmodified compressive tectonic features [e.g., *Withers and Neumann*, 2001].

8.4. Glacial Features

Another possible explanation of the circumferential features is that they are related to morainal/ice-margin features. A glacial explanation has been advanced for the formation of thumbprint terrain [*Lucchitta*, 1981; *Rossbacher*, 1985; *Lucchitta et al.*, 1987; *Scott and Underwood*, 1991; *Scott et al.*, 1992; *Kargel and Strom*, 1992; *Kargel et al.*, 1995]. As shown in Figure 10, there are areas of thumbprint terrain that are located in the middle of the zone of circumferential features in southern Utopia. On the basis of the morphology and distribution of thumbprint terrain and other structures, several workers have suggested the former presence of large ice sheets in the northern hemisphere of Mars [*Lucchitta et al.*, 1986; *Chapman*, 1994; *Kargel et al.*, 1995]. The lack of associated glacial flow features such as drumlins in the northern plains seems inconsistent with widespread glacial activity. Drumlins are streamlined mounds of glacial till that have elongated teardrop shapes in plan view [*Benn and Evans*, 1998]. The absence of drumlins does not rule out a glacial explanation, for a glacial body in the northern hemisphere may have been cold-based for much of its evolution [e.g., *Kargel et al.*, 1995]. However, the lack of drumlins highlights the general lack of features related to mass ice movement and scour in the interior of the Northern Plains. In addition, because ice experiences a drop in plasticity with decreasing temperature [*Glen*, 1955; *Goldsby et al.*, 2001], the current temperature regime on Mars would tend to inhibit glacial flow. This does not exclude the

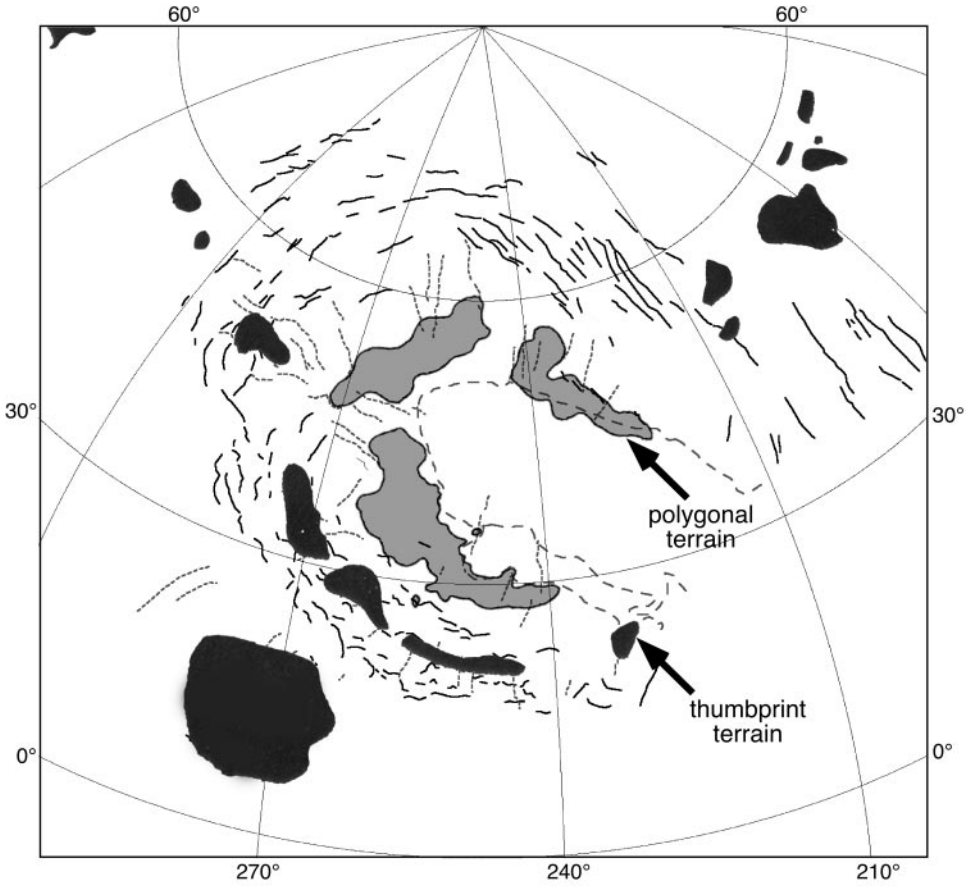

Figure 10. Map showing distribution of thumbprint terrain and polygonal terrain superposed on map showing distribution of linear features from Figure 1. Thumbprint terrain is shown as dark shaded regions as mapped by *Kargel et al.* [1995]. The lightly shaded regions are outcrops of polygonal terrain as mapped by *McGill* [1989].

possibility of glacial activity at periods of high obliquity or more temperate paleoclimatic conditions but highlights the need for a greater understanding of ice deformation mechanisms [*Goldsby et al.*, 2001] under possible Martian paleoclimates before the viability of a glacial explanation can be verified.

8.5. Open Water Features

Parker et al. [1989] presented evidence for as many as seven contacts between the northern plains and southern uplands, which were interpreted to be highstands of a former ocean. On Earth, wave-cut platforms and associated landforms result from direct coupling of wind and the open water surface [*Duane et al.*, 1972; *Swift et al.*, 1972, 1973; *Stubblefield et al.*, 1975; *Swift*, 1975; *Rice*, 1994]. Although wave erosion can occur relatively quickly, an extensive sequence of wave-cut platforms almost certainly requires extended periods of warmer, wetter climate on Mars. The morphology of terrestrial wave-cut platforms is controlled by such factors as the shoreline gradient, tidal range, wave strength, and bedrock composition [*Komar*, 1976]. Studies of terrestrial platforms indicate that there is a natural limit to the width [*Bradley*, 1958] and cross-platform gradient [*Zeuner*, 1952; *Fleming*, 1965; *Zenkowitch*, 1967; *Bradley and Griggs*, 1976]. The extreme width and low cross-platform gradient of the circumferential features in Utopia suggest that if they were related to a former standing body of water, other factors may have influenced their formation. These additional factors include the possibility that they represent a transgressive or regressive sequence of platform formation or perhaps that they are more similar to polar shorelines (see discussion below). A potentially analogous distribution of features is observed in the sand sheet on the Middle Atlantic Bight (Figure 11). First-order morphologic characteristics of this continental shelf region include cuestas and nearly horizontal terraces separated by more steeply inclined scarps. These terraces are interpreted to represent periods of Holocene transgression where the equilibrium shore-face profile has translated shoreward [*Swift et al.*, 1973]. Superimposed on these first-order features is ridge and swale topography, consisting of depositional sand ridges up to 10 m high that extended for tens of kilometers. The ridges are subparallel and form systems that are often at high angles to one another (Figure 11). The geographic distribution of these features in plan view is reminiscent of the distribution of circumferential features observed in Utopia (Figure 1).

8.6. Ice-Dominated Bodies of Water

A second possible analog for the circumferential features includes the extremely wide, near-horizontal platforms that are common in high-latitude regions on Earth. Known as strandflats, they are up to 50–60 km wide and have extremely low cross-platform gradients [e.g., *Evers*, 1962; *Benn and Evans*, 1998]. There have been many theories advanced for their formation, but many workers have highlighted the importance of frost shattering [*Nansen*, 1904, 1922; *Larsen and Holtedahl*, 1985; *Guilcher et al.*, 1994]. Frost action resulting from recurrent freeze-thaw cycles is an effective geomorphologic agent and is considered to be a key component of rapid coastal cliff recession and platform extension in polar seas [*Hansom*, 1983; *Matthews et al.*, 1986]. The most extensive strandflats are found in areas sheltered from wave erosion [e.g., *Hansom*, 1983]. An ice foot, or accumulation of sea ice frozen onto the shoreline, inhibits erosion by wave action

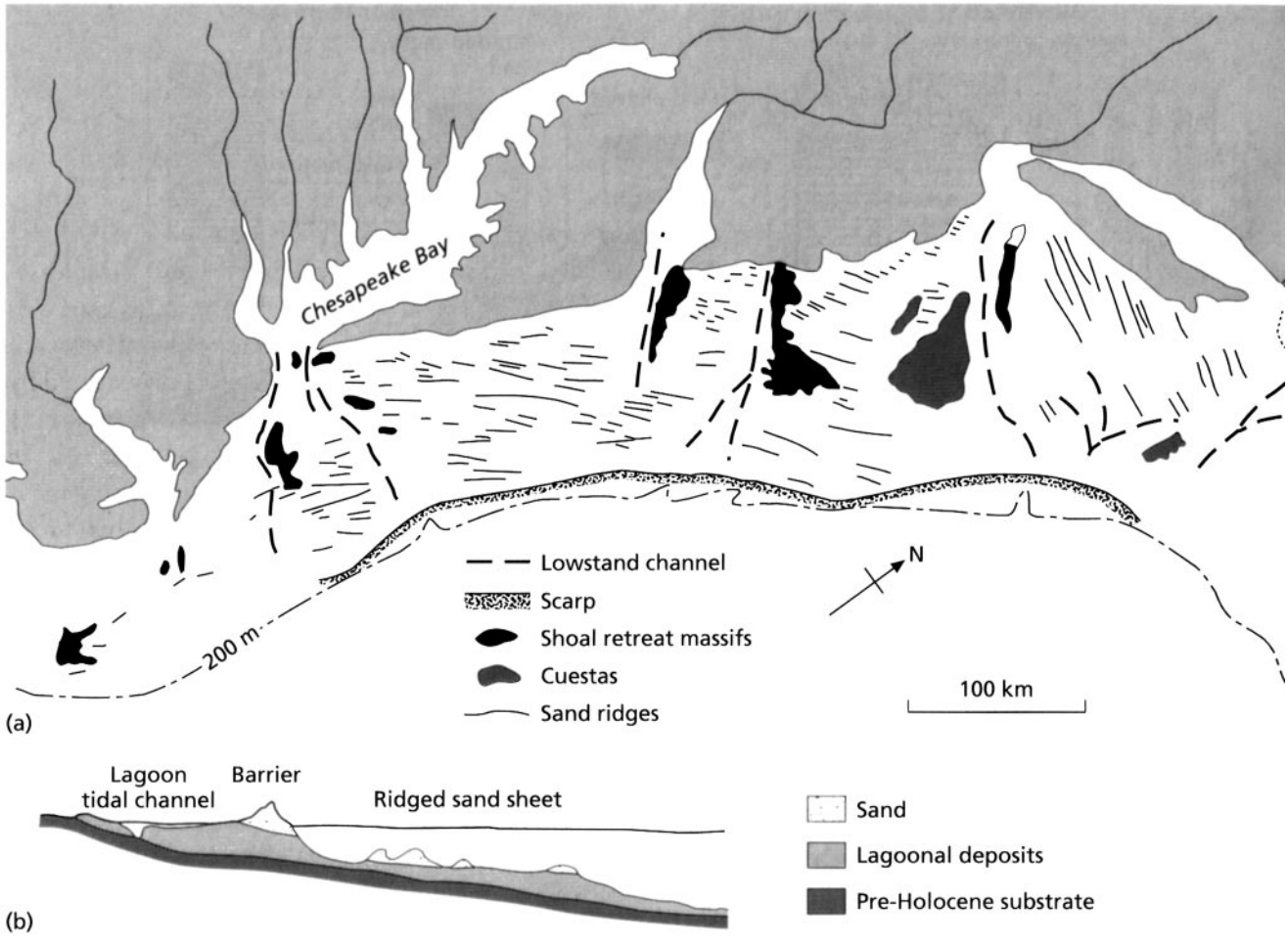

Figure 11. (a) Morphology of the Middle Atlantic Bight of the eastern continental shelf of North America showing features of relict and transgressive origins. The distribution of linear features resembles the distribution of circumferential features in Utopia Basin (see Figure 1). (b) Section across shelf to show transgressive barrier and progressively abandoned shelf sand ridges. (Figure from *Leeder* [1999] after *Swift et al.* [1973] and *Swift* [1974]. Reprinted with permission from Blackwell Science.) According to *Swift et al.* [1973], the sand ridges are typically 2–4 km apart and up to 10 m high.

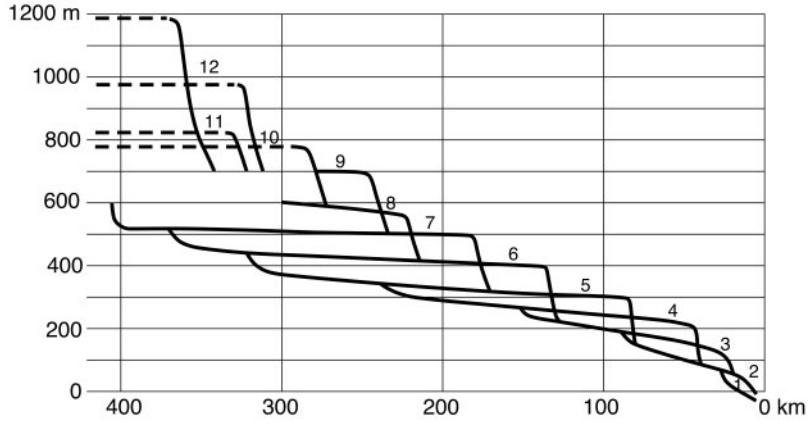

Figure 12. Idealized profile of the erosion generations of the Scandes to the east, in the Province of Västerbotten, north Sweden (figure from *Evers* [1962]). Each terraced step is a strandflat. Note that the scale of the figure is delineated in kilometers on the horizontal axis and in meters on the vertical axis.

during freeze periods but may increase the potential for frost shattering at the base of coastal cliffs [*Nansen*, 1922; *Feyling-Hanssen*, 1953; *Nielsen*, 1979]. Exposure of the coastline to wave action during thaw periods may increase the rate of platform formation by facilitating the removal of debris [*Matthews et al.*, 1986]. An idealized cross section of terrestrial strandflat generations is given in Figure 12. Note that the sequence of landforms shown is of similar scale to the circumferential features shown in Utopia [see also *Rice*, 2000].

9. Discussion

We now investigate the applicability of terrestrial and planetary analogs as candidate processes to explain the nature of the circumferential and radial ridges and linear slope anomalies mapped here. On the basis of our review, there are at least two potential terrestrial analogs to the circumferential features in Utopia. Shoreline processes in terrestrial periglacial shore environments can create features that are of similar size and scale to the Martian features. A similar distribution of longitudinal bed forms could also be formed through a regressive oceanic sequence. Both of these possible analogs require the presence of a significant standing body of water. There are a variety of features in Utopia Basin that have been interpreted as morphological indicators of water/ice. These include smooth infilled crater floors, channel deposits in and around the basin, and possible shoreline terraces and lineations [*Scott et al.*, 1992, 1995]. Other more enigmatic terrain that may be related to water or ground ice interaction in the Utopia region includes thermokarst [*Carr and Schaber*, 1977], thumbprint terrain [*Rossbacher and Jusdon*, 1981], polygonal terrain [*Pechmann*, 1980; *McGill*, 1986; *Hiesinger and Head*, 2000], rampart craters [*Carr et al.*, 1977], concentric crater fill [*Squyres*, 1979], table mountains [*Allen*, 1979], moberg hills and ridges [*Chapman*, 1994], and small cratered cones that might be pingos or pseudocraters [*Rossbacher and Jusdon*, 1981; *Frey and Jarosewich*, 1982]. On the basis of these features, several authors have suggested that Utopia Basin once contained ponded water/ice [*Parker et al.*, 1989, 1993; *Baker et al.*, 1991; *De Hon*, 1992; *Scott et al.*, 1992, 1995; *Chapman*, 1994; *Kargel et al.*, 1995].

On the basis of our review of planetary analogs, primary impact structures are unlikely to be preserved in Utopia Basin. Features associated with the modification, filling, and evolution of the basin appear to be more plausible. We find that tectonic wrinkle ridges appear to be the most likely analog to the concentric and radial features described in Utopia. Recent observations made with MOLA suggest that the northern lowlands are underlain by a regional unit (Hr, Hesperian ridged plains) containing a basin-wide system of subparallel wrinkle ridges and arches [*Head et al.*, 2001a, 2001b]. The presence of such an underlying ridged plains unit would divide the Martian hydrologic cycle into two distinct time frames: early Mars (Noachian) and post-Early Hesperian. Hydrologic modeling suggests that if Mars is or was water-rich and global temperatures were above freezing, then large bodies of water could have existed on its surface [*Gulick et al.*, 1997; *Clifford and Parker*, 1999; *Carr*, 2000]. These conditions may have been met in the Noachian with higher expected heat flows [*Schubert et al.*, 1992; *Zuber et al.*, 2000], higher erosion rates [*Carr*, 1992; *Craddock and Maxwell*, 1993; *Craddock et al.*, 1997], and the formation of valley networks [e.g., *Carr*, 1983; *Squyres and Kasting*, 1994], all of which possibly support a warmer, wetter climate [e.g., *Sagan et al.*, 1973; *Pollack et al.*, 1987]. However, with the exception of a few outcrops of Noachian-aged units [*Greeley and Guest*, 1987; *Scott and Tanaka*, 1986] and a population of quasi-circular depressions that may be buried impact structures [*Frey et al.*, 2001], most traces of this period of evolution in the northern plains appear to be buried under a substantial thickness of Early Hesperian volcanic deposits [*Head et al.*, 2001a, 2001b]. Given the inaccessibility of this time period, we shift our attention to activity that has occurred since the Early Hesperian.

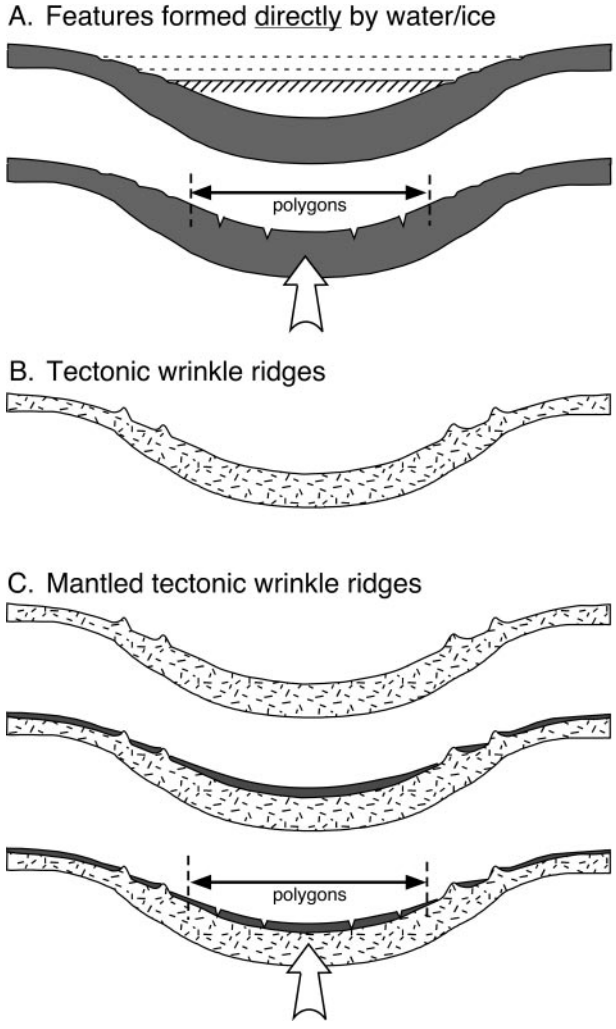

Figure 13. (a) Schematic profile of Utopia Basin showing a basement consisting of a sedimentary layer. In this first end-member scenario the top image shows a large standing body of water/ice impinging directly on the surface to create circumferential features. The bottom frame shows tectonic rebound following removal of the water load, resulting in formation of polygonal terrain. (b) This second end-member scenario shows the formation of ridges as wrinkle ridges resulting from tectonic deformation of the substrate. (c) This intermediate scenario shows thinner sedimentary layer overlying Hr basement deformed by wrinkle ridges. Note that the wrinkle ridges have been incompletely mantled. Again, rebound of the basin following removal of water/ice load initiates formation of polygonal terrain. Although not depicted here, the overlying sedimentary layer itself appears to have been deposited subaqueously.

Two end-member models for the formation of the ridges might be considered on the basis of previous hypotheses. First, *Parker et al.* [1989, 1993] interpreted similar features to be related to the stillstands of the margins of former standing bodies of water. In this scenario (Figure 13a), shoreline processes at the margins of a standing body of water produced structures now preserved as contacts and morphologic features. In this hypothesis, additional parallel features would be due to

variations in the level of water/ice [*Parker et al.*, 1989, 1993]; receding levels might produce parallel linear slope anomalies [e.g., *Head et al.*, 1999a]. This first scenario (Figure 13a) shows a thick sedimentary unit covering the floor of Utopia Basin. If the northern hemisphere of Mars ever contained an ocean, the smaller subbasins in the northern hemisphere would have filled first in the early stages of an ocean-filling event and may also have been partially flooded later in Martian evolution through subsequent outflows. An interpretation of the circumferential features described in this work that is consistent with observations of the characteristics of these features is that they represent a recessional sequence of a northern ocean. The residence time of such an ocean is indeterminate, although its eventual recession would be inevitable given the current Martian climate. Utopia Basin lies at lower latitudes than the North Polar Basin, so if the recession was largely through sublimation driven by insolation, Utopia would have been the site of net loss of water from the northern ocean. Water would have spilled over the saddle in the unnamed ridge to the north from the North Polar Basin into Utopia to replace what was lost as long as the two basins were in communication. In Figure 13a a retreating layer of water/ice is shown directly impinging upon the sedimentary layers, resulting in large circumferential terraces. This process would have continued until the water dropped to an elevation of about −4350 m, at which point the two basins would have no longer been in communication and the recessional geometry would have changed. Perhaps the remaining ice-dominated body of water grounded, froze solid, and retreated by sublimation. Subsequently, once the recession had gone to completion and the water was removed, the basin would then isostatically rebound. The explanation of polygonal terrain favored by *Hiesinger and Head* [2000] is formation through tectonic rebound following removal of a load. In this scenario the candidate for this transient load is water/ice. The geometry of the resulting state of stress induced by the rebound is strongly dependent on the lateral extent of the former load relative to the curvature of the planet [e.g., *Banerdt et al.*, 1992]; however, extensional stresses would be expected in the center of the basin as a result of the uplift [*Brotchie and Silvester*, 1969; *Solomon and Head*, 1979]. This isostatic extension may account for the formation of the polygonal terrain in the center of Utopia Basin. Later volcanic activity in Elysium activated a series of megalahars [*Christiansen*, 1989] that deposited volcanic material in the lowermost portions of Utopia Basin. This infilling buried the polygons that formed in the very bottom of Utopia and accounts for the horseshoe-shaped distribution of polygonal terrain presently observed in the basin (Figure 10).

A second end-member scenario would have the linear slope anomaly formation owing solely to wrinkle-ridge-related tectonic structure [e.g., *Withers and Neumann*, 2001] (Figure 13b). In this case, regional stresses from Tharsis and related areas deformed the northern lowlands to produce wrinkle ridges that account for the observed features and linear slope anomalies. This end-member model seems unlikely to fully account for the characteristics of the linear slope anomalies because of the differences in spacing, height, and patterns between the features in the northern lowlands and wrinkle ridges outside of the northern lowlands, documented in this research and by *Head et al.* [2001a, 2001b]. In addition, the presence of Late Hesperian sedimentary layers (the Vastitas Borealis Formation) in the northern lowlands strongly suggests that some sedimentary processes have modified any preexisting wrinkle-ridged surface.

Our examination of the characteristics of these features and related structures and texture in Utopia Basin leads us to a third alternative interpretation, lying between these two end-members. In this scenario (Figure 13c) we follow the interpretation of *Head et al.* [2001a, 2001b] and *Kreslavsky and Head* [2001], who conclude that the shallow basement of Utopia Basin is a thick volcanic unit emplaced in the Early Hesperian. Wrinkle ridges then formed in the middle part of the Hesperian in the volcanic unit due to basin subsidence, similar to the manner in which lunar mare ridges formed [*Maxwell*, 1978]. During the Late Hesperian, extensive outflow channels debouched repeatedly into the northern lowlands [e.g., *Rotto and Tanaka*, 1995; *Carr*, 1996; *Ivanov and Head*, 2001] to produce the Late Hesperian Vastitas Borealis Formation [e.g., *Tanaka and Scott*, 1987; *Kreslavsky and Head*, 1999, 2000]. Analysis of the roughness characteristics of the Vastitas Borealis Formation [*Kreslavsky and Head*, 1999, 2001] shows that its characteristics can be explained with the addition of a minimum of ∼100 m thickness of sediment on top of a typical Hesperian wrinkle-ridged plains surface [*Head et al.*, 2001a, 2001b; *Kreslavsky and Head*, 2001]. In this scenario (Figure 13c), water emplaced during the formation of the outflow channels in the Lower Hesperian flooded the basin (floored by Early Hesperian wrinkle-ridged plains) and deposited sediment that would ultimately form the Vastitas Borealis Formation. The thickness of sedimentary cover in Utopia is variable but thickens toward the basin center. The underlying ridged plains unit is incompletely covered with sedimentary material, so that some surface expression of the ridges remains. Depending on the degree of backfill, a mantled ridge might appear as a smaller ridge or as a bench-like terrace. Thus partially mantled wrinkle ridges may account for both the ridge and bench-like morphologies observed in this work. In addition to the general concept of the flooding of the northern lowlands by the outflow channels, several workers have specifically suggested that the overlying sedimentary layer in Utopia was water deposited [e.g. *Lucchitta et al.*, 1986; *McGill and Hills*, 1992]. Thumbprint terrain could be interpreted as features associated with recession of ice, representing the solidification of the water emplaced during the Late Hesperian basin flooding and its sublimation and retreat. Although the majority of linear features identified in this work appear to be tectonic structures modified by sedimentary processes, the possibility that some subset of the circumferential features in southern Utopia mapped in Figure 1 may have been formed by the direct action of water/ice has not been ruled out. Again, following the removal of the water/ice load, the surface isostatically rebounds, resulting in the formation of polygonal terrain in the center of the basin. Finally, in the Amazonian deposits from the Elysium area were emplaced on the basin floor, draping the southeastern margin and burying the polygonal terrain on the lowermost portion of the basin floor.

Is there evidence in high-resolution images for features related to the margins of areas where emplacement of water is likely to have occurred in the Late Hesperian? An initial investigation of a small suite of very high resolution MOC images that were specifically targeted at shoreline features previously identified in lower-resolution Viking images [*Scott et al.*, 1992; *Parker et al.*, 1993] did not reveal any features that have an obvious or unambiguous littoral origin [*Malin and Edgett*, 1999]. The absence of obvious shoreline indicators in the MOC images thus far reported is difficult to reconcile with the evidence for emplacement of a regional sedimentary unit, although *Malin and Edgett* [1999] note that it is usually difficult to identify paleocoastlines even on Earth from satellite or aerial photographs alone. The search for evidence of primary emplacement processes in the MOC images is further complicated by the unusual small-scale surface textures observed in Utopia [*Arvidson et al.*, 1979; *Zimbelman et al.*, 1989] and the northern hemisphere that coincide with a latitudinally dependant, small-scale smoothing effect observed in the MOLA topography [*Kreslavsky and Head*, 1999]. This latitudinal trend may indicate the deposition of a thin veneer of smooth material at high latitudes in the Late Amazonian.

Given the ephemeral nature of most terrestrial shoreline deposits and long-wavelength, low-amplitude submarine sedimentary struc-

tures, it is possible that many of the fine details have been eroded. For example, the Middle Atlantic Bight (Figure 11) consists of ridge and swale deposits superimposed on larger terraces and cuestas, as stated previously. As erosion progresses, the smaller ridges that are composed of unconsolidated sediments would preferentially be eroded.

In ongoing studies we are now turning our attention to the assessment of variations in the thickness of the sedimentary layer overlying the Hesperian ridged plains, its contact with units around the edge of the northern lowlands, and its relation to styles of modification of wrinkle ridges within the basin. These studies should cast further light on directions of sediment sources, styles of sediment emplacement, and the nature and evolution of the overlying medium (e.g., water, ice, or water transitioning to ice and subliming away).

10. Conclusions

New MOLA topographic data have revealed the general morphology of Utopia Basin and its interior deposits in unprecedented detail. Using these data, we have documented the nature of the basin and its internal structure. The MOLA data support the earlier interpretation [*McGill*, 1989] of Utopia as the site of an ancient impact basin and conclusively show that it is a broad, circular depression ~3200 km in diameter. We find two classes of linear features within the interior, one radial and the other circumferential to Utopia Basin. We consider two end-member hypotheses for these features, one in which they are related to shoreline and recessional features [*Parker et al.*, 1989, 1993; see also *Chapman*, 1994; *Kargel et al.*, 1995; *Scott et al.*, 1992, 1995] and one in which they are tectonic wrinkle-ridge structures [*Withers and Neumann*, 2001]. We conclude that neither end-member hypothesis accounts for all of the observations. We find that an intermediate model best explains the observations. In this model, sedimentary deposits were emplaced on top of Early Hesperian wrinkle-ridged volcanic plains in the Late Hesperian, during the period of outflow channel formation. These sedimentary deposits partially buried and obscured the pervasive wrinkle-ridge system and modified typical wrinkle-ridge cross-sectional shapes to those that are observed today. Subsequent studies should cast further light on sources of sediment, styles of sediment emplacement, and the nature and evolution of the overlying medium. In particular, these studies should focus on the nature, extent, residence time, and fate of the aqueous episode that appears to be necessary to explain the outflow channels and the sedimentary deposit of the Vastitas Borealis Formation.

On the basis of our analyses, the history of Utopia Basin can be outlined as follows:

1. Basin formation: Utopia Basin formed as a major impact structure in the Noachian period [*McGill*, 1989].
2. Early modification and fill: Gravity data strongly suggest that the basin underwent significant modification compared to Hellas Basin (Figure 1b) and was filled with material of sedimentary and volcanic origin [*Zuber et al.*, 2000].
3. Volcanic flooding: In the Early Hesperian, a unit of volcanic flows hundreds of meters thick was emplaced [*Head et al.*, 2001a, 2001b], similar to deposits observed at this time outside the northern lowlands (the Early Hesperian ridged plains, Hr) [*Greeley and Guest*, 1987; *Scott and Tanaka*, 1986].
4. Wrinkle-ridge formation: Following the emplacement of the volcanic plains in the middle part of the Hesperian period, these plains were tectonically deformed, resulting in the formation of pervasive wrinkle-ridge systems throughout the northern plains [*Head et al.*, 2001a, 2001b; *Withers and Neumann*, 2001] and elsewhere [*Watters and Maxwell*, 1986; *Chicarro et al.*, 1985]. In Utopia Basin, both radial and concentric wrinkle ridges formed. The subtle northward tilt of the basin described by *McGill* [2001] formed no later than mid-Late Hesperian.
5. Aqueous flooding and sediment deposition: In the Late Hesperian, effluents from outflow channels debouched into the northern lowlands, producing sedimentary deposits which mantle the underlying wrinkle-ridged plains to depths of at least 100 m on the average. These deposits (the Vastitas Borealis Formation) obscured and modified the wrinkle ridges to produce the characteristics of the linear features that we see today [*Head and Kreslavsky*, 2000; *Head et al.*, 2001a, 2001b].
6. Loss of flooding effluents: In the latest Hesperian, water associated with the emplacement of the outflow channels disappeared; on the basis of the nature of the modification of the ridges, their altitude distribution, and associated features such as the thumbprint terrain, it is likely that any water froze and retreated [e.g., *Chapman*, 1994; *Kargel et al.*, 1995].
7. Rebound of the basin floor: Following the removal of a load, most plausibly the loss of the water load associated with the earlier flooding, the basin rebounded, forming the polygonal terrain on the central part of the floor [e.g., *Hiesinger and Head*, 2000].
8. Emplacement of Amazonian Elysium deposits: Following formation of the polygonal terrain, lava flows and lahar-like deposits were emplaced from the Elysium rise in the Early Amazonian [*Greeley and Guest*, 1987; *Tanaka et al.*, 1992], draping the southeastern basin margin and covering the lowermost reaches of the basin floor (Figures 9 and 10) [*Christiansen*, 1989; *Tanaka et al.*, 1992; *Ivanov and Head*, 2001; *Russell and Head*, 2001].
9. Formation of a thin sedimentary veneer: In the latter part of the Amazonian a latitude-dependent sedimentary veneer modified the upper surface of the Vastitas Borealis Formation, obscuring the primary texture and structure of that unit [*Kreslavsky and Head*, 2000].

Acknowledgments. We would like to thank Misha Kreslavsky, Stephan Pratt, Peter Neivert, and Molly McCanta for their assistance and advice. We are also grateful for the helpful and constructive reviews by Victor Baker and an anonymous reviewer. This research was partially supported by a grant from the Mars Global Surveyor program to J.W.H.

References

Allen, C. C., Volcano-ice interactions on Mars, *J. Geophys. Res.*, *84*, 8048–8059, 1979.

Arvidson, R., E. Guinness, and S. Lee, Differential aeolian redistribution rates on Mars, *Science*, *278*, 533–535, 1979.

Baker, V. R., *The Channels of Mars*, 198 pp., Univ. of Tex. Press, Austin, 1982.

Baker, V. R., R. G. Strom, V. C. Gulick, J. S. Kargel, G. Komatsu, and V. S. Kale, Ancient oceans, ice sheets and the hydrological cycle on Mars, *Nature*, *352*, 589–594, 1991.

Baldwin, R. B., *The Measure of the Moon*, 488 pp., Univ. of Chicago Press, Chicago, Ill., 1963.

Banerdt, W. B., M. P. Golombek, and K. L. Tanaka, Stress and tectonics on Mars, in *Mars*, edited by H. H. Kieffer et al., pp. 249–297, Univ. of Ariz. Press, Tuscon, 1992.

Baulig, H., Peneplains and pediplains, *Geol. Soc. Am. Bull.*, *68*, 913–930, 1957.

Benn, D. I., and D. J. A. Evans, *Glaciers and Glaciation*, 734 pp., Oxford Univ. Press, New York, 1998.

Bradley, W. C., Submarine abrasion and wave-cut platforms, *Geol. Soc. Am. Bull.*, *69*, 967–974, 1958.

Bradley, W. C., and G. B. Griggs, Form, genesis, and deformation of central California wave-cut platforms, *Geol. Soc. Am. Bull.*, *87*, 443–449, 1976.

Brotchie, J. F., and R. Silvester, On crustal flexure, *J. Geophys. Res.*, *74*, 5240–5252, 1969.

Carr, M. H., Formation of Martian flood features by release of water from confined aquifers, *J. Geophys. Res.*, *84*, 2995–3007, 1979.

Carr, M. H., The stability of streams and lakes on Mars, *Icarus*, *56*, 476–495, 1983.
Carr, M. H., Post-Noachian erosion rates: Implications for Mars climate change (abstract), *Lunar Planet. Sci.*, *XXIII*, 205–206, 1992.
Carr, M. H., *Water on Mars*, 229 pp., Oxford Univ. Press, New York, 1996.
Carr, M. H., Martian oceans, valleys and climate, *Astron. Geophys.*, *141*, 20–26, 2000.
Carr, M. H., and G. G. Schaber, Martian permafrost features, *J. Geophys. Res.*, *82*, 4055–4065, 1977.
Carr, M. H., L. S. Crumpler, J. A. Cutts, R. Greeley, J. E. Guest, and H. Masursky, Martian impact craters and emplacement of ejecta by surface flow, *J. Geophys. Res.*, *82*, 4055–4056, 1977.
Chapman, M. G., Evidence, age, and thickness of a frozen paleolake in Utopia Planitia, Mars, *Icarus*, *109*, 393–406, 1994.
Chicarro, S. F., P. H. Schultz, and P. Masson, Global and regional ridge patterns on Mars, *Icarus*, *63*, 153–174, 1985.
Christiansen, E. H., Lahars in the Elysium region of Mars, *Geology*, *17*, 203–206, 1989.
Clifford, S. M., A model for the hydrologic and climatic behavior of water on Mars, *J. Geophys. Res.*, *98*, 10,973–11,016, 1993.
Clifford, S. M., and T. J. Parker, Hydraulic and thermal arguments regarding the existence and fate of a primordial Martian ocean (abstract), *Lunar Planet. Sci.* [CD-ROM], *XXX*, abstract 1619, 1999.
Coradini, M., and E. Flamini, A thermodynamical study of the Martian permafrost, *J. Geophys. Res.*, *84*, 8115–8130, 1979.
Craddock, R. A., and T. A. Maxwell, Geomorphic evolution of the Martian highlands through ancient fluvial processes, *J. Geophys. Res.*, *98*, 3453–3468, 1993.
Craddock, R. A., T. A. Maxwell, and A. D. Howard, Crater morphometry and modification in the Sinus Sabaeus and Margaritifer Sinus regions of Mars, *J. Geophys. Res.*, *102*, 13,321–13,340, 1997.
De Hon, R. A., Martian lake basins and lacustrine plains, *Earth Moon Planets*, *56*, 95–122, 1992.
Dreibus, G., and H. Wänke, Volatiles on Earth and Mars: A comparison, *Icarus*, *71*, 225–240, 1987.
Duane, D. B., M. E. Field, E. P. Meisburger, D. J. P. Swift, and S. J. Williams, Linear shoals in the Atlantic inner continental shelf, Florida to Long Island, in *Shelf Sediment Transport Process and Patterns*, edited by D. J. P. Swift, D. B. Duane, and O. H. Pilkey, pp. 447–498, Van Nostrand Reinhold, New York, 1972.
Evers, W., The problem of coastal genesis, with special reference to the "strandflat," the "banks," or "grounds," and "deep channels" of the Norwegian and Greenland coasts, *J. Geol.*, *70*, 621–630, 1962.
Feyling-Hanssen, R. W., Brief account of the ice-foot, *Norsk. Geogr. Tidsskr.*, *14*, 1–4, 1953.
Fleming, N. C., Form and relation to present sea level of Pleistocene marine erosion features, *J. Geol.*, *73*, 799–811, 1965.
Frey, H., and M. Jarosewich, Subkilometer Martian volcanoes: Properties and possible terrestrial analogs, *J. Geophys. Res.*, *87*, 9867–9879, 1982.
Frey, H., S. Sakimoto, and J. Roark, MOLA topographic structure of the Isidis and Utopia impact basins (abstract), *Lunar Planet. Sci.* [CD-ROM], *XXX*, abstract 1500, 1999.
Frey, H. V., K. M. Shockey, E. L. Frey, J. H. Roark, and S. E. H. Sakimoto, A very large population of likely buried impact basins in the northern lowlands of Mars revealed by MOLA data (abstract), *Lunar Planet. Sci.* [CD-ROM], *XXXII*, abstract 1680, 2001.
Glen, J. W., The creep of polycrystalline ice, *Proc. R. Soc. London, Ser. A.*, *228*, 519–538, 1955.
Goldsby, D. L., D. L. Kohlstedt, and R. Pappalardo, A composite flow law for water ice for use in modeling of glaciers, polar caps, and icy planetary interiors (abstract), *Lunar Planet. Sci.* [CD-ROM], *XXXII*, abstract 2067, 2001.
Golombek, M. P., J. B. Plescia, and B. J. Franklin, Faulting and folding in the formation of planetary wrinkle ridges, *Proc. Lunar Planet. Sci. Conf. 21st*, 679–693, 1991.
Greeley, R., Release of juvenile water on Mars: Estimated amounts and timing associated with volcanism, *Science*, *236*, 1653–1654, 1987.
Greeley, R., and J. E. Guest, Geologic map of the eastern equatorial regions of Mars, scale 1:15,000,000, *U.S. Geol. Surv. Misc. Invest. Ser. Map, I-1802-B*, 1987.
Greeley, R., J. E. Klemaszewski, and R. Wagner, Galileo views of the geology of Callisto, *Planet. Space Sci.*, *48*, 829–853, 2000.
Guilcher, A., J.-C. Bodéré, A. Coudé, J. D. Handom, A. Moign, and J.-P. Peulvast, The strandflat problem in five high latitude countries, in *Cold Climate Landforms*, edited by D. J. A. Evans, pp. 351–393, John Wiley, New York, 1994.
Gulick, V. C., D. Tyler, C. P. McKay, and R. M. Haberle, Episodic ocean-induced CO_2 greenhouse on Mars: Implications for fluvial valley formation, *Icarus*, *130*, 68–86, 1997.
Hansom, J. D., Shore-platform development in the South Shetland Islands, Antarctica, *Mar. Geol.*, *53*, 211–229, 1983.
Hartmann, W. K., and C. A. Wood, Concentric structures surrounding lunar basins, *Commun. Lunar Planet. Lab.*, *1*, 55–66, 1962.
Head, J. W., and M. A. Kreslavsky, Northern lowlands on Mars: New evidence for formation and evolution from detrended MOLA topography (abstract), in *Vernadsky Institute—Brown University Microsymposium*, vol. 32, pp. 52–53, Vernadsky Inst., Moscow, 2000.
Head, J. W., M. Kreslavsky, H. Hiesinger, M. Ivanov, S. Pratt, N. Seibert, D. E. Smith, and M. T. Zuber, Oceans in the past history of Mars: Tests for their presence using Mars Orbiter Laser Altimeter (MOLA) data, *Geophys. Res. Lett.*, *25*, 4401–4404, 1998.
Head, J. W., H. Hiesinger, M. A. Ivanov, M. A. Kreslavsky, S. Pratt, and B. J. Thomson, Possible ancient oceans on Mars: Evidence from Mars Orbiter Laser Altimeter data, *Science*, *286*, 2134–2137, 1999a.
Head, J. W., E. M. Stewart, and S. Pratt, Analysis of global and regional slope distributions for Venus (abstract), *Lunar Planet. Sci.* [CD-ROM], *XXX*, abstract 1264, 1999b.
Head, J. W., M. A. Kreslavsky, and S. Pratt, Northern lowlands of Mars: Evidence for widespread volcanic flooding and tectonic deformation in the Hesperian period, *J. Geophys. Res.*, in press, 2001a.
Head, J. W., M. A. Kreslavsky, and S. Pratt, Northern lowlands on Mars: Evidence for widespread volcanic flooding and tectonic deformation in the Early Hesperian (abstract), *Lunar Planet. Sci.* [CD-ROM], *XXXII*, abstract 1063, 2001b.
Hess, S. L., R. M. Henry, C. B. Leary, J. A. Ryan, and J. E. Tillman, Meteorological results from the surface of Mars: Viking 2, *J. Geophys. Res.*, *82*, 4559–4574, 1977.
Hiesinger, H., and J. W. Head, III, Characteristics and origin of the polygonal terrain in southern Utopia Planitia, Mars: Results from Mars Orbiter Laser Altimeter and Mars Orbiter Camera data, *J. Geophys. Res.*, *105*, 11,999–12,022, 2000.
Ivanov, M., and J. W. Head, Chryse Planitia, Mars: Topographic configuration, outflow channel continuity and sequence, and tests for hypothesized ancient bodies of water using Mars Orbiter Laser Altimeter (MOLA) data, *J. Geophys. Res.*, *106*, 3275–3295, 2001.
Jöns, H.-P., Sedimentary basins and mud flows in the northern lowlands of Mars (abstract), *Lunar Planet. Sci.*, *XV*, 417–418, 1984.
Jöns, H.-P., Late sedimentation and late sediments in the northern lowlands on Mars (abstract), *Lunar Planet. Sci.*, *XVI*, 414–415, 1985.
Jöns, H.-P., Das Relief des Mars: Versuch einer zusammenfassenden Übersicht, *Geol. Rundsch.*, *79*, 131–164, 1990.
Kargel, J. S., and R. G. Strom, Ancient glaciation on Mars, *Geology*, *20*, 3–7, 1992.
Kargel, J. S., V. R. Baker, J. E. Begét, J. F. Lockwood, T. L. Péwé, J. S. Shaw, and R. G. Strom, Evidence of continental glaciation in the Martian northern plains, *J. Geophys. Res.*, *100*, 5351–5368, 1995.
Kieffer, H. H., T. Z Martin, A. R. Peterfreund, B. M. Jakosky, E. D. Mine, and F. D. Palluconi, Thermal and albedo mapping of Mars during the primary mission, *J. Geophys. Res.*, *82*, 4249–4292, 1977.
Komar, P. D., *Beach Processes and Sedimentation*, 429 pp., Prentice-Hall, Old Tappan, N. J., 1976.
Kreslavsky, M. A., and J. W. Head, III, Kilometer-scale slopes on Mars and their correlation with geologic units: Initial results from Mars Orbiter Laser Altimeter (MOLA) data, *J. Geophys. Res.*, *104*, 21,911–21,924, 1999.
Kreslavsky, M. A., and J. W. Head, III, Stealth craters in the northern lowlands of Mars: Evidence for a buried Early-Hesperian-aged unit (abstract), *Lunar Planet. Sci.* [CD-ROM], *XXXII*, abstract 1001, 2001.
Larsen, E., and H. Holtedahl, The Norwegian strandflat: A reconsideration of its age and origin, *Nor. Geol. Tidsskr.*, *65*, 247–254, 1985.
Leeder, M., *Sedimentology and Sedimentary Basins*, 592 pp., Blackwell Sci., Malden, Mass., 1999.
Lucchitta, B. K., Mars and Earth: Comparison of cold-climate features, *Icarus*, *45*, 264–303, 1981.
Lucchitta, B. K., Ice in the northern plains: Relic of a frozen ocean? (abstract), in *MSATT Workshop on the Martian Northern Plains, LPI Tech. Rep.*, *93-04*, pp. 9–10, Lunar and Planet. Inst., Houston, Tex., 1993.
Lucchitta, B. K., H. M. Ferguson, and C. Summers, Sedimentary deposits in the northern lowland plains, Mars, *Proc. Lunar Planet. Sci. Conf. 17th, Part 1, J. Geophys. Res.*, *91*, E166–E174, 1986.
Lucchitta, B. K., H. M. Ferguson, and C. Summers, Northern sinks on Mars? (abstract), *LPI Tech. Rep.*, *87-02*, pp. 32–33, Lunar and Planet. Inst., Houston, Tex., 1987.
Malin, M. C., and K. S. Edgett, Oceans or seas in the Martian northern lowlands: High resolution imaging tests of proposed coastlines, *Geophys. Res. Lett.*, *26*, 3049–3052, 1999.
Malin, M. C., and K. S. Edgett, Evidence for recent groundwater seepage and surface runoff on Mars, *Science*, *288*, 2330–2335, 2000.
Mars Channel Working Group, Channels and valleys on Mars, *Geol. Soc. Am. Bull.*, *94*, 1035–1054, 1983.

Masursky, H., An overview of geologic results from Mariner 9, *J. Geophys. Res.*, *78*, 4009–4030, 1973.
Masursky, H., and N. L. Crabill, Search for the Viking 2 lander site, *Science*, *194*, 62–68, 1976.
Matthews, J. A., A. G. Dawson, and R. A. Shakesby, Lake shoreline development, frost weathering and rock platform erosion in an alpine periglacial environment, Jotunheimen, south Norway, *Boreas*, *15*, 33–50, 1986.
Maxwell, T. A., Origin of multi-ring basin ridge systems: An upper limit to elastic deformation based on a finite element model, *Proc. Lunar Planet Sci. Conf. 9th*, 3541–3559, 1978.
McCauley, J. F., M. H. Carr, J. A. Cutts, W. K. Hartmann, H. Masursky, D. J. Milton, R. P. Sharp, and D. E. Wilhelms, Preliminary Mariner 9 report of the geology of Mars, *Icarus*, *17*, 289–327, 1972.
McGill, G. E., The giant polygons of Utopia, northern Martian plains, *Geophys. Res. Lett.*, *13*, 705–708, 1986.
McGill, G. E., Buried topography of Utopia, Mars: Persistence of a giant impact depression, *J. Geophys. Res.*, *94*, 2753–2759, 1989.
McGill, G. E., The Utopia Basin revisited: Regional slope and shorelines from MOLA profiles, *Geophys. Res. Lett.*, *28*, 411–414, 2001.
McGill, G. E., and L. S. Hills, Origin of the giant Martian polygons, *J. Geophys. Res.*, *97*, 2633–2647, 1992.
McKinnon, W. B., and H. J. Melosh, Evolution of planetary lithospheres: Evidence from the multiringed structures on Ganymede and Callisto, *Icarus*, *44*, 454–471, 1980.
Mellon, M. T., and B. M. Jakosky, The distribution and behavior of Martian ground ice during past and present epochs, *J. Geophys. Res.*, *100*, 11,781–11,799, 1995.
Melosh, H. J., *Impact Cratering: A Geologic Process*, 245 pp., Oxford Univ. Press, New York, 1989.
Milton, D. J., Water and processes of degradation in the Martian landscape, *J. Geophys. Res.*, *78*, 4037–4047, 1973.
Nansen, F., The bathymetrical features of the North polar seas, in *The Norwegian North Polar Expedition 1893–1896: Scientific Results*, *Vol. IV*, edited by F. Nansen, pp. 1–232, Copp, Clark, Mississauga, Ont., Canada, 1904.
Nansen, F., The strandflat and isostacy, *Skr. Vid. Selsk. Krist. Mat. Naturvid.*, *2*, 1–313, 1922.
Nielsen, N., Ice-foot processes: Observations of erosion on a rocky coast, Disko, West Greenland, *Z. Geomorphol.*, *23*, 321–331, 1979.
Parker, T. J., R. S. Saunders, and D. M. Schneeberger, Transitional morphology in West Deuteronilus Mensae, Mars: Implications for modification of the lowland/upland boundary, *Icarus*, *82*, 111–145, 1989.
Parker, T. J., D. S. Gorsline, R. S. Saunders, D. C. Pieri, and D. M. Schneeberger, Coastal geomorphology of the Martian northern plains, *J. Geophys. Res.*, *98*, 11,061–11,078, 1993.
Pechmann, J. C., The origin of polygonal troughs on the northern plains of Mars, *Icarus*, *42*, 185–210, 1980.
Pike, R. J., and P. D. Spudis, Basin-ring spacing on the Moon, Mercury, and Mars, *Earth Moon Planets*, *39*, 129–194, 1987.
Plescia, J. B., Wrinkle ridges of Arcadia Planitia. Mars, *J. Geophys. Res.*, *98*, 15,049–15,059, 1993.
Pollack, J. B., J. F. Kasting, S. M. Richardson, and K. Poliakoff, The case for a warm, wet climate on early Mars, *Icarus*, *71*, 203–224, 1987.
Rice, J. W., Terrestrial polar beach processes: Martian paleolake analogues (abstract), *Lunar Planet. Sci.*, *XXV*, 1125–1126, 1994.
Rice, Jr. J. W., Flooding and ponding on Mars: Field observations and insights from the polar realms of the Earth (abstract), *Lunar Planet. Sci.* [CD-ROM], *XXXI*, abstract 2067, 2000.
Rossbacher, L. A., Ground ice models for the distribution and evolution of curvilinear landforms on Mars, in *Models of Geomorphology*, edited by M. J. Woldenburg, pp. 343–372, Allen and Unwin, Concord, Mass., 1985.
Rossbacher, L. A., and S. Jusdon, Ground ice on Mars: Inventory, distribution, and resulting landforms, *Icarus*, *45*, 39–59, 1981.
Rotto, S., and K. L. Tanaka, Geologic/geomorphic map of the Chryse Planitia region of Mars, scale 1:5,000,000, *U.S. Geol. Surv. Misc. Invest. Ser. Map, I-2441*, 1995.
Russell, P. S., and J. W. Head, The Elysium/Utopia flows: Characteristics from topography and a model of emplacement (abstract), *Lunar Planet. Sci.* [CD-ROM], *XXXII*, abstract 1040, 2001.
Sagan, C., O. B. Toon, and P. J. Gierasch, Climatic change on Mars, *Science*, *181*, 1045–1049, 1973.
Schubert, G., S. C. Solomon, D. L. Turcotte, M. J. Drake, and N. L. Sleep, Origin and thermal evolution of Mars, in *Mars*, edited by H. H. Kieffer et al., pp. 147–183, Univ. of Ariz. Press, Tuscon, 1992.
Schultz, R. A., and H. V. Frey, A new survey of multiring impact basins of Mars, *J. Geophys. Res.*, *95*, 14,175–14,189, 1990.
Scott, D. H., and K. L. Tanaka, Geologic map of the western equatorial regions of Mars, scale 1:15,000,000, *U.S. Geol. Surv. Misc. Invest. Ser. Map, I-1802-A*, 1986.
Scott, D. H., and J. R. Underwood, Jr., Mottled terrain: A continuing Martian enigma, *Proc. Lunar Planet. Sci. Conf. 21st*, 627–634, 1991.
Scott, D. H., M. G. Chapman, J. W. Rice, Jr., and J. M. Dohm, New evidence of lacustrine basins on Mars: Amazonis and Utopia Planitiae, *Proc. Lunar Planet Sci. Conf. 22nd*, 53–62, 1992.
Scott, D. H., J. M. Dohm, and J. W. Rice, Jr., Map of Mars showing channels and possible paleolake basins, scale 1:30,000,000, *U.S. Geol. Surv. Misc. Invest. Ser. Map, I-2461*, 1995.
Sharp, R. P., and M. C. Malin, Channels of Mars, *Geol. Soc. Am. Bull.*, *86*, 593–609, 1975.
Sharpton, V. L., and J.W. Head, III, Analysis of regional slope characteristics on Venus and Earth, *J. Geophys. Res.*, *90*, 3733–3740, 1985.
Sharpton, V. L., and J. W. Head, III, A comparison of the regional slope characteristics of Venus and Earth: Implications for geologic processes on Venus, *J. Geophys. Res.*, *91*, 7545–7554, 1986.
Smith, D. E., et al., Topography of the northern hemisphere of Mars from the Mars Orbiter Laser Altimeter, *Science*, *279*, 1686–1692, 1998.
Smith, D. E., et al., The global topography of Mars and implications for surface evolution, *Science*, *284*, 1495–1503, 1999.
Solomon, S. C., and J. W. Head, Vertical movement in mare basins: Relation to mare emplacement, basin tectonics, and lunar thermal history, *J. Geophys. Res.*, *84*, 1667–1682, 1979.
Solomon, S. C., and J. W. Head, Lunar mascon basins: Lava filling, tectonics and evolution of the lithosphere, *Rev. Geophys.*, *18*, 107–141, 1980.
Spudis, P. D., *The Geology of Multi-Ring Impact Basins*, 263 pp., Cambridge Univ. Press, New York, 1993.
Squyres, S. W., The distribution of lobate debris aprons and similar flows on Mars, *J. Geophys. Res.*, *84*, 8087–8096, 1979.
Squyres, S. W., and M. H. Carr, Geomorphic evidence for the distribution of ground ice on Mars, *Science*, *231*, 249–252, 1986.
Squyres, S. W., and J. F. Kasting, Early Mars: How warm and how wet?, *Science*, *265*, 744–748, 1994.
Stubblefield, W. L., J. W. Lavelle, and D. J. P. Swift, Sediment response to the present hydraulic regime on the central New Jersey Shelf, *J. Sediment. Petrol.*, *45*, 337–358, 1975.
Swift, D. J. P., Continental shelf sedimentation, in *The Geology of Continental Margins*, edited by C. A. Burk and C. L. Drake, pp. 117–135, Springer-Verlag, New York, 1974.
Swift, D. J. P., Tidal sand ridges and shoal-retreat massifs, *Mar. Geol.*, *18*, 105–134, 1975.
Swift, D. P., D. P. Duane, and T. F. McKinney, Ridge and swale topography of the Middle Atlantic Bight, North America: Secular response to the Holocene hydraulic regime, *Mar. Geol.*, *15*, 227–247, 1973.
Swift, D. J. P., J. W. Kofoed, F. P. Saulsbury, and P. Sears, Holocene evolution of the shelf surface, central and southern Atlantic shelf of North America, in *Shelf Sediment Transport Process and Patterns*, edited by D. J. P. Swift, D. B. Duane, and O. H. Pilkey, pp. 499–574, Van Nostrand Reinhold, New York, 1972.
Tanaka, K. L., and D. H. Scott, Geologic map of the polar regions of Mars, scale 1:15,000,000, *U.S. Geol. Surv. Misc. Invest. Ser. Map, I-1802-C*, 1987.
Tanaka, K. L., M. G. Chapman, and D. H. Scott, Geologic map of the Elysium region of Mars, scale 1:5,000,000, *U. S. Geol. Surv. Misc. Invest. Ser. Map, I-2147*, 1992.
Thomson, B. J., and J. W. Head, III, Utopia Basin, Mars: A new assessment using Mars Orbiter Laser Altimeter (MOLA) data (abstract), *Lunar Planet. Sci.* [CD-ROM], *XXX*, abstract 1894, 1999.
U.S. Geological Survey, *Mars Digital Terrain Models* [CD-ROM], vol. 7, *Global Topography*, NASA, Greenbelt, Md., 1993.
Ward, W. R., B. C. Murray, and M. C. Malin, Climatic variations of Mars, 2, Evolution of carbon dioxide atmosphere and polar caps, *J. Geophys. Res.*, *79*, 3387–3395, 1974.
Washburn, A. L., Instrumental observations of mass-wasting in the Mesters Vig District, Northeast Greenland, *Medd. Grønl.*, *166*, 318 pp., 1967.
Watters, T. R., Origin of periodically spaced wrinkle ridges on the Tharsis Plateau of Mars, *J. Geophys. Res.*, *96*, 15,599–15,616, 1991.
Watters, T. R., Compressional tectonism on Mars, *J. Geophys. Res.*, *98*, 17,049–17,060, 1993.
Watters, T. R., and T. A. Maxwell, Orientations, relative age, and extent of the Tharsis Plateau ridge system, *J. Geophys. Res.*, *91*, 8113–8125, 1986.
Wilhelms, D. E., Comparison of Martian and lunar multi-ringed circular basins, *J. Geophys. Res.*, *78*, 4084–4095, 1973.
Withers, P., and G. A. Neumann, Enigmatic northern plains of Mars, *Nature*, *410*, 651, 2001.

Wood, C. A., and J. W. Head, Comparison of impact basins on Mercury, Mars and the Moon, *Proc. Lunar Sci. Conf. 7th*, 3629–3651, 1976.

Witbeck, N. E., and J. R. Underwood, Jr., Geologic mapping in the Cydonia region of Mars, *NASA Tech. Memo.*, *NASA TM 86246*, 327–329, 1983.

Wu, S. S. C., Topographic map of the eastern region of Mars, scale 1:15,000,000, *U.S. Geol. Surv. Map, I-2160*, 1991.

Yung, Y. L., J. Wen, J. P. Pinto, M. Allen, K. K. Pierce, and S. Paulsen, HDO in the Martian atmosphere: Implications for the abundance of crustal water, *Icarus*, *76*, 146–159, 1988.

Zenkowitch, V. P., *Processes of Coastal Development*, 738 pp., Oliver and Boyd, White Plains, N. Y., 1967.

Zeuner, F. E., Pleistocene shore-lines, *Geol. Rundsch.*, *40*, 39–50, 1952.

Zimbelman, J. R., S. M. Clifford, and S. H. Williams, Concentric crater fill on Mars: An aeolian alternative to ice-rich mass wasting, *Proc. Lunar Sci. Conf. 19th*, 397–407, 1989.

Zuber, M. T., et al., Internal structure and early thermal evolution of Mars from Mars Global Surveyor topography and gravity, *Science*, *287*, 1788–1793, 2000.

J. W. Head, III and B. J. Thomson, Department of Geological Sciences, Brown University, Box 1846, Providence, RI 02912, USA (james_head_iii@brown.edu; bthomson@porter.geo.brown.edu)

(Received August 14, 2000; revised May 8, 2001;
accepted May 16, 2001.)